Numerical modeling of progressive failure and its implications to spreads in sensitive clays

Ariane LOCAT – Corresponding author

Département de génie civil et de génie des eaux, Université Laval

Pavillon Adrien-Pouliot, 1065 av. de la Médecine, Québec, Qc, Canada G1V 0A6

Tel : 1 418 656 2992 Fax: 1 418 656 2928

ariane.locat@gci.ulaval.ca

Hans Petter JOSTAD

Norwegian Geotechnical Institute

P.O. Box. 3930 Ullevål Stadion, N-0806, Olso, Norway

Tel: +47 22 02 30 49 Fax: +47 22 23 04 48

hans.petter.jostad@ngi.no

Serge LEROUEIL

Département de génie civil et de génie des eaux, Université Laval

Pavillon Adrien-Pouliot, 1065 av. de la Médecine, Québec, Qc, Canada G1V 0A6

Tel : 1 418 656 2131 ext : 2601 Fax: 1 418 656 2928

serge.leroueil.@gci.ulaval.ca

Abstract

Spreads are a type of large landslides occurring in sensitive clays. Stability analyses using limit equilibrium method give too large factors of safety and are therefore not applicable to this type of landslide. The progressive failure mechanism is believed to explain the initiation and propagation of the failure surface and the dislocation of the soil mass in horsts and grabens, typical of spreads. A numerical method is presented in order to identify the parameters influencing progressive failure and to validate the application of this mechanism to spreads. The method evaluates the stresses acting in the slope before failure and models the initiation and propagation of the progressive failure. It is demonstrated that high, steep slopes, with large earth pressure ratio at rest are more susceptible to progressive failure and the latter propagates over a large distance. Failure is more likely to occur when soil with high brittleness is involved. Soil with low strength at large deformation induces failure propagation over a larger distance. Eastern Canadian clays can exhibit a high sensitivity and a large brittleness during shear and are susceptible to progressive failure which explains the occurrence of spreads in these soils.

Key words: Progressive failure, spreads, sensitive clays, stresses in slopes, brittleness.

Résumé

Les étalements sont de grands glissements de terrain survenant dans les argiles sensibles. Les méthodes d'analyse de la stabilité utilisant la méthode à l'équilibre limite donnent des coefficients de sécurité élevés et ne peuvent s'appliquer à ces glissements. Le mécanisme de rupture progressive expliquerait l'initiation et la propagation de la surface de rupture et la dislocation du sol en horst et en grabens, typiques aux étalements. Une méthode numérique est présentée afin d'identifier les paramètres influençant la rupture progressive et de valider son application aux étalements. Cette méthode évalue les contraintes présentes initialement dans le talus et modélise l'initiation et la propagation de la rupture progressive. Il est démontré que les hautes pentes, fortement inclinées ayant un coefficient de pression des terres au repos élevé sont susceptibles à la rupture progressive et que celle-ci se propage sur une grande distance. La rupture est favorisée par un sol ayant une grande fragilité lors du cisaillement. Une faible résistance à grande-déformation du sol favorise une grande distance de propagation. Les argiles de l'est du Canada, pouvant présenter une forte sensibilité et une grande fragilité lors du cisaillement, sont donc susceptibles à la rupture progressive et celle-ci explique l'occurrence d'étalements dans ces sols.

Mots-clés : Rupture progressive, étalements, argiles sensibles, contraintes dans les pentes, fragilité.

1. Introduction

In sensitive clays, large landslides, classified as spreads by Cruden and Varnes (1996), involve the translation and dislocation of the soil mass in blocks having horst and graben shapes (Figure 1). These landslides occur in clay deposits and are generally triggered by natural phenomena arising from the gradual erosion going on near the toe of the slope (Demers et al. 2013). One case was reported to be triggered by pile driving in the municipality of Ste-Madeleine-de-Rigaud (Carson 1979). In several cases, the failure surface was located with piezocone tests performed inside the debris of the landslide (Locat 2007; Locat et al. 2008, 2011*b*; Fortin-Rhéaume 2013). It was observed that the failure surface or shear zone generally starts near the toe of the slope and progresses quasi-horizontally into the deposit. The soil above the shear zone then dislocates into several blocks of more or less intact material having horst and graben shapes, which results in a spread as illustrated on Figure 1. Angle of the tips of horsts has value around 60° from the horizontal, corresponding to active failure occurring by lateral stress reduction during shearing for Canadian sensitive clays (Locat et al. 2011*a*). This angle is similar to the one observed in undrained triaxial compression tests on intact overconsolidated natural clays. The dislocation of the soil mass is believed to occur quite rapidly, as indicated by witnesses of the 1989 Saint-Liguori spread (Grondin et Demers 1996) and can have disastrous consequences, as exemplify by the tragic death of a family of four in the 2010 Saint-Jude landslide (Locat et al. 2011*b*). The rapidity of these events indicates that the water pressures generated during these landslides do not have the time to dissipate during failure. Dislocation of the soil mass in horsts and grabens is therefore believed to occur essentially in undrained conditions. These morphologic features in the crater of spreads distinguish them from other large landslides occurring in sensitive clays such as flows leaving empty craters (Demers et al. 2013). Karlsrud et al. (1984) noted that combination of different types of landslides can also occur in on event. The Mink Creek landslide, in British Columbia (Geertsema et al. 2006), is a good example where flow and spread occurred successively in one landslide event.

Clays from Eastern Canada can be sensitive and can show a strain-softening behaviour in undrained conditions, and may therefore be susceptible to progressive failure (Lo 1972, Leroueil et al. 1983; Locat 2007; Ouehb 2007; Locat et al. 2008; Fortin-Rhéaume 2013). Spreads in Eastern Canada sensitive clays occur suddenly, cover large areas and conventional limit equilibrium stability analyses give safety factors above unity for these landslides (Demers et al. 2013). Previous studies (Odenstad 1951, Carson 1977 and 1979b) have considered spreads and suggested failure mechanism for this particular type of landslides. They mainly focused on the dislocation of the soil mass in horsts and grabens, without explaining the progression of the quasi-horizontal failure surface under those blocks. Recent studies (Locat et al. 2008; Locat et al. 2011*a*; Locat 2012; Quinn et al. 2011 and 2012) brought forward the hypothesis that these landslides can be explained by progressive failure.

In the progressive failure mechanism the soil exhibits a stress-strain behaviour of the soil, including post peak strain-softening, to propagate shear stresses and deformations along a shear zone (Terzaghi and Peck 1948; Skempton 1964; Bishop 1967 and 1971; Bjerrum 1967; Christian and Whitman 1969; Bernander 2000, 2008 and 2011; Urciuoli et al. 2007). In the case of spreads, according to Locat et al. (2011*a*) and Quinn et al. (2011 and 2012), failure is initiated near the toe of the slope and propagates essentially horizontally into the intact deposit, reducing horizontal stresses in the deposit (upward progressive failure as described by Locat et al. 2011*a*). If the horizontal total stress becomes less than the active resistance of the soil mass above the shear zone, the soil mass in the slope may break into blocks of more or less intact material having horst and graben shapes. As failure propagates inside the deposit, a larger zone may reach active failure leading to the formation of a succession of horsts and grabens. Spreads are therefore the results of progressive failure and active failure of an extensive part of the soil mass above the failure surface.

According to Locat et al. (2011*a*), the following conditions and stages for initiation and propagation of progressive failure in clay deposits, triggered by phenomena like erosion at the toe of the slope, are:

- The soil must have a post peak strain-softening behaviour during undrained shear deformation including a large-deformation shear strength (τ_{ld}) lower than the initial shear stress (τ_o) near the toe of the slope.
- A critical disturbance ($\Delta\sigma_{crU}$) has to be applied so that the peak shear strength (τ_p) can be exceeded. The soil will then soften and progressive failure can be initiated.
- Once the failure is initiated, it propagates under no additional disturbance than $\Delta\sigma_{crU}$ and the large-deformation shear strength (τ_{ld}) is gradually mobilised along the failure surface. The failure propagates further inside the deposit, where the shear stress (τ_o) is lower, and stops when $\Delta\sigma_{crU}$ is completely distributed along the shear zone.
- During failure propagation, the horizontal stresses in the soil mass above the shear zone decreases and might reach the undrained active strength of the soil (σ_{Act}) along a section of the deposit and lead to the formation of multiple horsts and grabens along that section, resulting in a spread.

The progressive failure mechanism has been numerically studied in the context of failure initiated near the toe of clay slopes for which the entire soil mass has a strain-softening behaviour by Lo (1972), Lo and Lee (1973*a* and *b*) and Kovacevic et al. (2004 and 2007). In addition, it has also been applied to the context of large landslides in long gently inclined clay slopes by Andresen and Jostad (2004 and 2007) and Gylland et al. (2010) with the finite element program BIFURC, developed at the Norwegian Geotechnical Institute. The program has been applied to slopes, formed of sensitive clays, in which progressive failure is initiated upslope and progresses downslope causing passive failure (downward progressive failure according to Bernander 2000, 2008 and 2011 and Locat et al. 2011*a*). Quinn et al. (2011 and 2012) use an approach involving fracture mechanics, introduced by Palmer and Rice (1973) for clay slopes, to understand large landslides occurring in sensitive clays. In addition, Locat et al. (2011*a*) extended Bernander (2000, 2008 and 2011) progressive failure mechanism to spreads in order to introduce a failure mechanism explaining these landslides. These studies indicated that initiation and propagation of progressive failure in Eastern Canadian clay slopes could explain the occurrence of spreads. However, progressive failure analysis has never been used to study spreads occurring in sensitive clays.

Bjerrum (1967), studying progressive failure in overconsolidated plastic clays and clay shales, as well as Lo and Lee (1973*a* and *b*) and Kovacevic et al. (2004 and 2007), modeling progressive failure in excavated clay slopes, stated that initial geometry and earth pressure ratio at rest (K_o) influence progressive failure initiated near the toe of slopes. In particular, Lo and Lee (1973*a* and *b*) showed that an increase in slope height and inclination increases the proportion of the failure surface along which the strength of the soil has fallen down to the large deformation shear strength.. It was observed that K_o departing from unity resulted in larger zones in the slope where failure occurred. Bernander (2000, 2008 and 2011), Bernander and Olofsson (1981*a* and *b*) and Gylland et al. (2010) showed that soils with higher sensitivity and lower stiffness increase the susceptibility of infinite slopes to progressive failure.

Quinn et al. (2011 and 2012) extended a model by Palmer and Rice (1973) using fracture mechanics to large landslides in sensitive clays. The fracture mechanism approach uses the fracture energy, defined by the area under the stress-displacement curve from the peak shear strength to the large-deformation shear strength, to explain the progressive failure propagation. In this mechanism, a given failure surface propagating over a critical distance may release sufficient strain energy to initiate a progressive failure propagating further inside the deposit. Quinn et al. (2011) deduced from fracture mechanism that brittleness influences the susceptibility to progressive failure initiation and the potential for large failure propagation.

According to the studies mentioned above, the factors influencing progressive failure initiation and propagation can be divided in two types regarding their influence: (*i*) those defining the initial stress in a slope prior to a landslide (initial slope geometry and K_o); and (*ii*) those defining the soil behaviour during progressive failure (strengths, brittleness and stiffness of the shear zone and soil mass above it). The objective of this study is to identify factors leading to progressive failure initiated near the toe of sensitive clay slopes that generate spreads and their influence on the initiation and extent of the failure. In order to achieve this objective, the finite element software PLAXIS 2D 2010 (PLAXIS Manuals 2011) is used to calculate the shear stresses in a slope before failure and the finite element program BIFURC (Jostad and Andresen 2002) is used to model progressive failure with the initial stresses from PLAXIS. The paper begins with a description of the numerical method used. The results of the study showing the effect of the stresses in slopes and soil behaviour on progressive failure are then presented. Finally, the results are discussed to get better understanding of the process and factors controlling spreads in sensitive clays.

2. Method

2.1. Definition of progressive failure

The progressive failure mechanism as described by Locat et al. (2011*a*) is illustrated on Figure 2. Figure 2a, presents the geometry of a slope having a height (H) and an inclination (θ) resulting from valley formation and is typical of Eastern Canadian slopes where spreads occur. In this case, the potential shear zone is represented as a dashed line in Figure 2a. In this schematic example, the potential failure surface is assumed to be horizontal and to start at the toe of the slope. This assumption is based on studies of spreads where the failure surface was located with piezocone tests (Locat 2007; Locat et al. 2008, 2011*b*; Fortin-Rhéaume 2013) and was found to be inclined close the horizontal. The initial shear stress ($\tau_o(x)$) along this potential failure surface and the average initial horizontal total stress ($\sigma_{xo}(x)$) above the potential failure surface before failure are shown by dashed lines on Figures 2b and c, respectively. The shear stress initially present in the slope is near zero away from the crest of the slope and is maximal at a point such as *A* ($\tau_{o\ max}$), under the slope. The average horizontal total stress ($\sigma_{xo}(x)$) is at its maximum value at the left boundary and begins to decrease at some distance behind the crest of the slope and reaches a minimum at the toe of the slope.

The movement of the soil mass during a spread is considered to be mainly horizontal and shear is assumed to be localised to the shear zone in which the failure surface develops. The behaviour of the potential shear zone is therefore considered to be similar to simple shear. In a progressive failure analysis, it is generally assumed that the soil exhibits strain-softening stress-strain behaviour with peak shear strength (τ_p) and a lower large deformation shear strength (τ_{ld}) (Bishop 1967 and 1971; Bjerum 1967; Lo 1972; Lo and Lee 1973a and b; Bernander 2000, 2008 and 2011; Leroueil et al. 2012). Strain-softening stress-displacement behaviour is therefore assumed for the shear zone, with peak shear strength (τ_p) and a large-deformation shear strength (τ_{ld}) reached at corresponding horizontal displacements δ_p and δ_{ld} respectively, as shown on Figure 2d. In addition, the soil above the potential failure surface or shear zone is considered to be elastic with an undrained active strength (σ_{Act}, Figure 2c).

Let us assume that, due to a small landslide near the toe of the slope (for example dashed line BC on Figure 2a), unloading initiates a shear zone at point *A*, where the initial shear stress is maximal ($\tau_{o\ max}$) and closer to the peak shear strength of the soil (τ_p) (time 1 on Figures 2e and f, arrow at point *A* is pointing in the failure propagation direction). Figures 2e and f show resulting distributions of the shear stress ($\tau_1(x)$) along the potential failure surface and the average horizontal total stress ($\sigma_1(x)$) above the potential failure surface at time 1. It can be seen that the peak shear strength is mobilised at point *b* and that the strength of the soil decreases between *b* and *A* (Figure 2e, curve $\tau_{x1}(x)$), following the post-peak softening stress-displacement behaviour of the soil (Figure 2d). According to horizontal equilibrium (Figure 3), the change in total horizontal stress ($\Delta\sigma_x$) corresponding to a change in shear stress during failure (τ_x - τ_o) over a length (L) along the potential shear zone can be calculated with the following equation:

$$[1]\ \Delta\sigma_x = \frac{\int_0^L (\tau_x - \tau_o)dL}{H_x}$$

where H_x is the height of the soil mass at a point *x* along the potential failure surface.

Further shear will decrease the shear strength at point *A* (Figure 2e) to the large-deformation shear strength. This loss of strength may lead to negative values of (τ_x - τ_o) in Equation 1 and of $\Delta\sigma_x$ at point *A*, indicating a decrease of resistance along the potential failure surface with increasing shear. According to Bernander (2000, 2008 and 2011) and Locat et al. (2011*a*), this defines a condition where the failure propagates in the shear zone under no additional unloading ($\Delta\sigma_x$) at point *A*. Thus, $\Delta\sigma_x$ at point *A* at time 1 on Figures 2e and f defines a critical maximum unloading stress ($\Delta\sigma_{crU}$) that can be applied at point *A* before initiation of instability along the potential failure surface. Initiation of instability is defined here as the maximum resisting unloading stress that the soil can offer under increasing shear (limit when $\Delta\sigma_x$ starts to decrease). Under further shear deformation, the soil loses strength as it continues to soften and progressive failure is initiated.

$\Delta\sigma_{crU}$ can be calculated by integrating the shear stress along the shear zone for increasing $\Delta\sigma_x$ to find the value where it starts to become negative according to Equation 1:

$$[2]\ \Delta\sigma_{crU} = \frac{\int_A^a (\tau_x - \tau_o)dx}{H_A}$$

where the distance between *A* and *a* defines the length of the shear zone when $\Delta\sigma_{crU}$ is applied and H_A is the height of the slope at point *A* (see Figure 2e and f). $\Delta\sigma_{crU}$ may physically be caused by a landslide, rapid unloading by erosion or excavation at point *A*. $\Delta\sigma_{res}$ represents the total horizontal stress at point *A* remaining after instability initiation.

If the critical unloading stress ($\Delta\sigma_{crU}$) defined above is reached, progressive failure is initiated and progresses inside the soil mass. Falling dominoes can be used as an analogy to progressive failure. The critical unlading stress initiating progressive failure can be picture as the fall of the first domino destabilising the nearby dominoes. Once the failure is initiated, the failure propagates in more stable ground away from the crest of the slope until the critical disturbing stress ($\Delta\sigma_{crU}$) is completely distributed along the shear zone (Time 2 on Figure 2g and h). The failure may propagate until equilibrium is established between the critical unloading stress and the shear stress along the shear zone. Figures 2g and h present the shear stress and average horizontal total stress (curves τ_{x2}(x) and σ_{x2}(x) respectively) once the failure has finished to propagate (time 2). The large-deformation shear strength (τ_{ld}) is now mobilised at point *A* and along a portion of the failure surface (curve τ_{x2}(x) on Figure 2g). The average horizontal total stress in the slope decreased as the failure propagated and is now at the undrained active strength (σ_{Act}) of the soil over a given length along the failure surface (curve σ_{x2}(x) Figure 2h). In order to redistribute the disturbance $\Delta\sigma_{crU}$ applied at point *A*, the shear zone progressed into the deposit up to point *a*', located at a distance where the effect of the unloading is negligible. The final propagation distance of the failure (L_f) is measured from point *A* to *b*', where the peak shear strength is mobilised at time 2. The retrogression distance of the failure (L_R) is measured from the crest of the slope before failure to point *b*'. At time 2, and possibly even before, the horizontal stress has reached the undrained active strength (σ_{Act}) over a given length along the failure surface. Under this failure process, as suggested by Locat et al. (2011a), the soil mass above the shear zone extends and dislocates into horsts and grabens that translate downslope, as they partly subside into the remoulded clay of the shear zone. Dislocation of the soil mass results from the propagation of the shear zone, and consequently active failure and lack of support from the remoulded shear zone. A crucial aspect of the failure mechanism presented herein is that failure propagation and dislocation of horsts and grabens are considered to be essentially independent processes. A detailed description of the failure mechanism used in this study is given by Locat et al. (2011a).

2.2. Assumptions and methods

In this study, the modeling of progressive failure is done in two steps: (*i*) calculation of initial stresses in the slope with the finite element software PLAXIS 2D 2010 (PLAXIS Manuals 2011) by unloading of a river valley; and (*ii*) modeling of the initiation and propagation of progressive failure with the finite element code BIFURC (Andresen and Jostad 2004 and 2007; Jostad and Andresen 2002). This section describes the assumptions and limitations of the methods of both calculation steps with their respective geometry, mesh, boundary conditions and constitutive soil models.

The modeling is done with the following assumptions and limitations:

- The slopes where spreads occur in Eastern Canada have been formed by river erosion and can generally be modeled as an unloading process of an initially horizontal deposit.
- The valley formation takes place over thousands of years and is considered as a drained process. As illustrated by Leroueil (2001), pore pressures near excavations made in Eastern Canada clay takes

only few months to few years to reach equilibrium, the assumption of drained conditions therefore seems valid.

- The failure surface was located with piezocone tests for several cases of spreads. In most of the studied cases, it starts near the toe of the initial slope and propagates almost horizontally into the deposit (Locat 2007; Locat et al. 2008; Fortin-Rhéaume 2013). It is therefore assumed in this study that the failure surface is horizontal and located at the elevation of the toe of the initial slope.
- During progressive failure:
    - The process is rapid and considered to be undrained.
    - Ground movement in a spread is generally translational with subsidence (Cruden and Varnes 1996). It will be assume here that shear strains are limited to a shear zone in which a potential failure surface may develop by progressive failure.
    - Soil layer above the shear zone is laterally unloaded (decrease of horizontal stress and corresponding change in horizontal displacement).
    - Uniform displacement over the height of the soil layer above the shear zone is assumed to simplify the numerical model.
    - The shear zone has a stress-strain-softening behaviour during shearing.
    - Uniform strain is assumed over the height (t) of the shear zone.
    - Elastic stress-strain behaviour is assigned to the soil layer above the shear zone.
    - No strain rate effect is taken into account.
    - No inertia effect is taken into account (quasi-static response).
    - The unloading triggering the failure may decrease as failure propagates (see section 2.4.3). This reduction might be explained by factors not taken into account in the present analyses, such as inertia effect, strain-rate effects, or geometrical changes of the soil mass (Andresen and Jostad 2004; and Gylland and Jostad 2010).

2.3. Evaluation of initial stresses in slopes

The finite element software PLAXIS 2D 2010 (PLAXIS Manuals 2011) is used to determine the stresses in a horizontal deposit where a river valley is being formed in drained conditions. The initial conditions are those conditions prevailing in the horizontal deposit before erosion and the results of this step are the stresses in the slope after valley formation, in particular the shear stresses along a horizontal surface at the elevation of the toe of the slope.

2.3.1. Geometry, mesh and boundary conditions

Before valley formation:

An example of geometry, mesh and boundary conditions before valley formation is presented in Figure 4a. Initially, before valley formation, the deposit is horizontal. The bottom of the model is at a depth 3H (H is the height of the considered slope and the depth to the lower boundary under the toe of the slope taken to be 2H). This is, of course a simplification and the depth of the lower boundary may be adjusted according to an actual case study. The model from the left boundary to the crest of the slope is 500 m long, which is considered long enough for the left boundary not to be affected by the valley formation occurring near the right boundary. The total length of the model is 500 m plus the horizontal length of the slope from its crest to its toe (L_s) plus H. The valley is assumed to be symmetric.

The mesh is made of triangular elements with 15 nodes and is refined near the final profile of the slope. The number of elements will vary according to the size of the model (a function of H and L_s). The left and right boundaries are fixed in the horizontal direction and the bottom boundary is fixed in both directions. The water table level follows the ground surface, which is a reasonable assumption in the Quebec climatic context.

<u>After valley formation:</u>

After valley formation, the elements forming the valley are deactivated from the model in drained conditions. The geometry, the mesh and the boundary conditions after valley formation are presented in Figure 4b. The slope has a height (H) and an inclination (θ). The bottom of the valley is horizontal and has a width that has been taken equal to 2H (1H in half-model).

The left, right and bottom boundaries are considered impervious. The ground water head (h) is adjusted to have zero water pressure at the ground surface along the top of the deposit, from the left boundary to the crest of the slope, and the bottom of the river valley. The slope itself is considered as a free boundary where water can flow freely.

2.3.2. Soil model and parameters

The Hardening Soil Model, available in PLAXIS, is used in the calculation of the initial shear stresses. Figure 5 shows the basic characteristics and input parameters of the model which are according to PLAXIS Manuals (2011):

- A reference tangent oedometer modulus during virgin loading (E_{oed}^{ref}, see Figure 5a);
- A reference secant Young modulus at 50% shear strength mobilisation (E_{50}^{ref}, see Figure 5b);
- A reference unloading / reloading modulus at 50% shear strength mobilisation (E_{ur}^{ref}, see Figure 5b);
- A hyperbolic stress-strain relationship for the axial strain (ε_1) and deviatoric stress (q) during shear defined by a failure ratio ($R_f = q_f/q_a$, see Figure 5b) of the ultimate deviatoric stress at failure (q_f) and the asymptotic value to which tends the relationship (q_a);
- A Poisson's ratio for unloading / reloading (ν'_{ur});
- Stress dependency for all stiffness parameters moduli (E), which follows expressions similar to:

$$[3]\ E = E^{ref}\left(\frac{\sigma'_i + a}{p_{ref} + a}\right)^m$$

where a is equal to a = c' cot ϕ', p_{ref} a reference pressure where the input reference modulus E^{ref} is valid, σ'_i is the stress, and exponent m is the amount of stress dependency;

- Failure parameters defining the Mohr-Coulomb criterion: cohesion (c), friction angle (ϕ'), and dilatation angle (ψ);
- Isotropic hardening connected to two plastic yield surfaces: (*i*) a cone hardening giving plastic strain controlled by increase of mobilised friction and (*ii*) a cap hardening giving plastic volumetric strain controlled by the preconsolidation stress (p'_c, see Figure 5c).

Readers are refered to PLAXIS manuals (2011) for detailed information on this soil model.

Parameters values for the Hardening Soil Model used in this study are presented in Table 1. The soil tangent oedometer modulus (E_{oed}^{ref}) value, for a reference pressure (p_{ref}) of 100 kPa, chosen in the present study is 21000 kPa. This value is representative of an Eastern Canadian clays with preconsolidation stress (σ'_p) of 233 kPa for p_{ref} of 100 kPa (according to Leroueil et al. 1983: $E_{oed} \approx 90\ \sigma'_p = 90 \times 233$ kPa ≈ 21000 kPa). The reference secant Young modulus at 50% shear strength mobilisation (E_{50}^{ref}) is taken to be equal to the tangent oedometer modulus (According to PLAXIS manuals 2011: $E_{50}^{ref} \approx E_{oed}^{ref} = 21000$ kPa) and the reference unloading / reloading modulus at 50% shear strength mobilisation (E_{ur}^{ref}) is taken to be equal to three times the reference secant Young modulus at 50% shear strength mobilisation (According to PLAXIS manuals 2011: $E_{ur}^{ref} = 3E_{50}^{ref} = 63000$ kPa). As indicated in PLAXIS manuals (2011), m should be equal to 1 for soft clays. A value of 0.9 for R_f has been chosen, which is the default value in Plaxis. The Poisson's ratio (ν'_{ur}) was taken equals to 0.25 since the soil is deforming in drained conditions. A cohesion (c') of 35 kPa and a friction angle (ϕ') of 35° have been kept constant throughout the analyses and chosen in order to keep the slope stable for the entire parametric study for which the maximum slope inclination and height are 30° and 30 m, respectfully. The dilatancy angle (ψ) has been taken equal to zero and the unit weight of the soil has been taken equal to 17 kN/m^3. The type of soil selected for the flow parameters is set to be very fine and, the hydraulic conductivity is assumed isotropic and equal to 10^{-9} m/s. The other parameters are set to the default values defined by PLAXIS (see PLAXIS Manuals 2011 and Table 1). The values described above have been kept constant throughout the analysis and their effect is considered to be negligible for this study.

2.3.3. Numerical method

Initial conditions:

The initial conditions in the horizontal deposit are calculated using the K_o procedure (see PLAXIS Manuals 2011). To observe the effect of K_o on progressive failure, K_{oi} values varying between 0.5 and 1.5 were used. These ranges of K_{oi} are large for sensitive clays and are chosen to make sure that the effect of K_{oi} is well taken into account in the analysis.

The initial pore water pressures are considered hydrostatic and calculated on the basis of the water table level.

Drained unloading:

To model the formation of the river valley, the cluster forming the river valley is deactivated in one step in drained conditions using the drained calculation option in PLAXIS (see PLAXIS Manuals 2011). In the same calculation, the water table level is put to the final ground surface and the boundary conditions described above are defined. The water pressures are calculated according to these conditions in a steady state ground water flow calculation (see PLAXIS Manuals 2011).

The horizontal shear stress (τ_o) along a horizontal section crossing the entire mesh at the river elevation (see dashed line on Figure 4b) is an output from the calculation. These shear stresses are used to calculate the corresponding average total horizontal stress (σ_{xo}) in the soil above the shear zone, with the following equation from horizontal equilibrium:

$$[5]\ \sigma_{xo\,j} = \frac{E_{j-1}}{H_{j-1}} + \frac{\Delta E_j}{H_j} = \sigma_{xo\,j-1} + \frac{\tau_{o\ average\ j} L_j}{H_j}$$

where j and j-1 are successive vertical sections separated by length L_j, ΔE_j is the change in horizontal force due to earth pressure in the soil above the shear zone over the length L_j, H_j is the height of the soil above the cross-section over which the average horizontal total stress σ_{xoj} applies and $\tau_{o\ average\ j}$ is the average shear stress along the length L_j (see Figure 6). Calculations are done from the left boundary to the toe of the slope.

2.4. Modeling progressive failure

Stresses calculated from the PLAXIS analysis are used as initial conditions in the analysis of progressive failure initiation and propagation with BIFURC. The numerical method of this progressive failure analysis is described in this section.

2.4.1. Element types, mesh and boundary conditions

The soil mass is divided into two different parts: (*i*) an upper soil layer, deforming laterally above (*ii*) a shear zone (Figure 7a). A horizontal, linear shear zone is presented on Figure 7 and is used in this study. A local coordinate system is used where the x- and z-axis are respectively oriented parallel and perpendicular to the ground surface and the potential failure surface (see Figure 7a).

Elements modeling the upper soil layer above the shear zone are 3-noded truss elements with two displacement degrees of freedom at the nodal points, δ_x and δ_z (Figure 7b). The height (H) of those elements may vary from node to node and defines the geometry of the problem along with the location of the nodes. Those elements may be subjected to loading or unloading in the x-direction. The displacement is assumed constant over the height of the elements.

The displacement δ_x along the interface at the top of the shear zone is modeled with 6-noded isoparametric (zero thickness) interface elements with two displacement degrees of freedom in the nodal points, δ_x and δ_z (Figure 7b).

The mesh is formed with one bottom layer of interface elements and a top layer of truss elements (see Figure 7c). The lower boundary of the mesh is fixed in both directions. The upper nodes of the interface elements are common with the nodes of the truss elements. As the interface elements represent the interface at the top of the shear zone, the height of the model is defined by the height of the truss elements. In all cases modeled in this study, the mesh has a length of 500 m and is divided in 1000 truss elements and 1000 interface elements of same length.

2.4.2. Constitutive soil models

In this study, the shear zone is assigned a strain-softening stress-strain behaviour as schematised in Figure 8a. The behaviour is defined by a peak shear strength (τ_p), a large-deformation strength (τ_{ld}) and corresponding shear strains (γ_p and γ_{ld}). The post-peak strength is assumed to decrease linearly with increasing shear strain. The hypothesis of this study is that the shear zone of thickness *t* deforms in conditions similar to an idealised direct simple shear tests (fixed bottom and horizontal shear stress applied at the top are assumed). The displacement along the interface at the top of the shear zone δ_x can be calculated from the shear strain γ_{zx} over the entire thickness of the shear zone:

[7] $\delta_x = \int_o^t \gamma_{zx} dz$

Considering uniform shear strain (γ_{zx}) distribution over the thickness of the shear zone and constant shear zone thickness (*t*), the horizontal displacement at the top of the shear zone is equal to:

[8] $\delta_x = \gamma_{zx} \times t$

The horizontal displacement when the peak shear strength of the soil is mobilised is thus equal to:

[9] $\delta_p = \gamma_p \times t$

In the post-peak domain, the strength of the soil decreases linearly to its large-deformation shear strength (τ_{ld}). The shear strain distribution is still considered uniform in the post peak behaviour and the displacement at which the large-deformation shear strength is mobilised can be calculated using:

[10] $\delta_{ld} = \gamma_{ld} \times t$

Using Equations 8 to 10, the stress-strain behaviour of the shear zone is converted to a stress-displacement curve input for the interface element representing the top of the shear zone of a given thickness *t* (Figure 8). The thickness of the shear zone is taken into account in the stress-displacement relationship input to the interface element, as shown on Figure 8. Therefore, the interface elements represent the interface at the top of the shear zone and have zero thickness in the numerical model.

The estimation of the shear zone thickness on a landslide scale is not easy to assess. Leroueil (2001) explains, using observations from various cases in different materials, that shear surfaces are generally surrounded by shear zones with a thickness varying from a few centimeters to a few decimeters, depending on the material and the displacement involved. In the present study, a shear zone thickness of 0.5 m is assumed. More research is needed to define the shear zone characteristics.

An example of a stress-strain behaviour used for this analysis is presented on Figure 9a and the soil parameters are summarized in Table 2. Peak shear strength (τ_p) of 70 kPa and large-deformation shear strength of 10 kPa (τ_{ld}) are used. These strengths were chosen as they enable to initiate and propagate a progressive failure in all the studied cases. Corresponding shear strains (γ_p and γ_{ld}) are 1% and 25%

respectively, which is consistent with the shear behaviour of Eastern Canadian clays and the end of a DSS test, respectively. Using the shear zone thickness (*t*) of 0.5m, it is possible to convert the stress-strain behaviour shown in Figure 9a into a stress-displacement behaviour needed as input in BIFURC (using Equations 8 to 10), as shown on Figure 9b. Displacements at the peak shear strength (δ_p) of 0.005 m and when the large-deformation shear strength is reached (δ_{ld}) of 0.125 m have been calculated and input in the model for the shear zone.

In this study the truss elements shown on Figures 7b and c represent the soil mass above the shear zone and are given a linear elastic behaviour. The lateral elastic strain along the x-axis (ε_x) for an element subjected to a change in horizontal stress ($\Delta\sigma_x$) can be calculated with a stiffness modulus (E_{el}) as shown by the following equation:

$$[6]\ \varepsilon_x = \varepsilon_x^e = \frac{\Delta\sigma_x}{E_{el}}$$

Very high strengths in compression and extension are given to these elements to avoid failure conditions. It is assumed in this study that the soil above the shear zone has a stiffness modulus (E_{el}) of 10500 kPa. This is about 3 times the average shear modulus ($G_{average}$) for the entire soil layer above the potential shear zone ($G_{average} \approx (\tau_p/\gamma_p) / 2 = (70\ \text{kPa}/0.01) / 2 = 3500\ \text{kPa}$). Although E_{el} varies with stress and OCR, it is considered constant in this analysis in order to isolate its effect.

To simplify the numerical model, these parameters have been considered constant along the potential failure surface. Table 2 summarises the soil parameters used in BIFURC. These parameters values are varied throughout the analysis in order to observe their influence on progressive failure, except when indicated otherwise.

2.4.3. Finite element procedure

In the progressive failure analysis, the calculations start from the initial state of stress previously calculated with PLAXIS. An external nodal load vector ($\mathbf{N}_{ext}$) is then applied at point *A* in increments (Figure 7). To vary this external load, the solution algorithm multiplies an input reference load vector (N_{ref}) having two degrees of freedom in each node (only a horizontal force in one node is applied here) to a load factor *p*:

[11] $\mathbf{N}_{\mathrm{ext}} = \mathrm{p}\mathbf{N}_{\mathrm{ref}}$

Starting from the initial state of stress, the program finds the corresponding nodal point displacement vector ($\mathbf{r}$) that satisfies equilibrium between the internal nodal force vector ($\mathbf{N}_{int}$) and the external force vector ($\mathbf{N}_{ext}$). $\mathbf{N}_{int}$ is given by the internal stresses in the soil mass and shear stress along the interface elements:

[12] $\mathbf{N}_{\mathrm{int}} = \int_{\mathrm{o}}^{\mathrm{L}} \mathbf{B}^{\mathrm{T}}\boldsymbol{\sigma}\mathrm{dx}$

where $\mathbf{B}$ is the matrix that gives the relationship between the strain vector and the nodal point displacement vector ($\mathbf{r}$) and $\boldsymbol{\sigma}$ is the stress vector containing the input initial stresses (shear stress and total horizontal stress) and the stress changes due to deformations along the x-direction. The above integral, over the entire length of the element (L), is solved numerically by loops over all elements in the model and numerical integration within each element. Equilibrium requires that:

[13] $\mathbf{N}_{\mathrm{ext}} = \mathbf{N}_{\mathrm{int}}$

For each load step, the displacement $\mathbf{r}$ is calculated by an iterative predictor-corrector procedure together with an arc-length control method. More details on the finite element procedure and the solution algorithm are given in the context of this study by Locat (2012). As a result, the program applies a load N_{ext}, decreasing the average horizontal total stress, and varies it automatically for each increment by varying the load factor *p* (see Equation 11), and thus increases the displacement. In doing so, the program follows the stress-displacement behaviour of the soil to propagate this additional load and evaluate the corresponding changes in stresses and displacement along the mesh.

Figure 10a gives an example of the variation of the load factor *p* as a function of the maximum displacement at the end of each increment at the node located at point *A*, where the unloading is applied. This node is a common to an interface element and a truss element (see nodal point *A*, Figure 7c). Figure 10b presents the shear stress along the potential failure surface for three specific increments. For the first 21 increments, the program increases the load factor at nodal point *A* to increase the horizontal displacement. As the load factor increases, the slope is being unloaded and shear progresses along the potential failure surface. As shear progresses, the interface element linked to nodal point *A*, as well as other interface elements nearby, reaches the peak shear strength and loses strength due the interface element strain-softening behaviour once the peak shear strength is mobilised. Under this loss of strength, the program needs to reduce the load factor in order to increase the displacement at nodal point *A* and to propagate the failure further, as seen after increment 21 (Figure 7a). This means that after increment 21, the interface element linked to nodal point *A*, as well as other interface elements nearby, loses strength due their strain-softening behaviour and the failure propagates with no additional disturbance than the unloading applied at increment 21. Increment 21 represents therefore the application of the critical unloading needed to initiate progressive failure ($\Delta\sigma_{crU}$) presented at time 1 on Figure 2. As failure progresses further along the potential failure surface in more stable ground, where the initial shear stress is lower, the program increases the load factor at the node at point *A* (increment 39, Figures 10a and b). The program is stopped at increment 66, when the load factor increases back to its maximal value, which is $\Delta\sigma_{crU}$, reached at increment 21. This indicates that the unloading applied at increment 21 ($\Delta\sigma_{crU}$) is fully distributed along the potential failure surface. As further unloading would be needed to propagate the failure over a larger distance, increment 66 represents the end of the failure extent when $\Delta\sigma_{crU}$ is applied. The critical unloading stress ($\Delta\sigma_{crU}$) and final extent of the failure shown for increment 66 in Figure 10b are therefore direct results of the numerical method. The decrease of the load factor after the application of $\Delta\sigma_{crU}$ has been reached may not be physically realistic in all situations and might be explained by factors not taken into account in the present analyses, as inertia effects, strain-rate effects, or geometrical changes of the failing soil mass (Andresen and Jostad, 2004).

3. Stresses in slopes

The first step of this progressive failure analysis is the calculation of the shear stresses along a potential failure surface in a slope formed by valley formation. The evaluation of these stresses is important as they form the basis of the entire analysis. The study has focused on the effect of the geometry of the slope and the initial earth pressure ratio at rest (K_{oi}) on the maximum shear stress along the potential failure surface ($\tau_{o\ max}$ see Figure 2b). The soil parameters used are as described in Section 2.3.2 and in Table 1.

In order to observe the combined effect of slope height, inclination and K_{oi} on the maximum shear stress along the potential failure surface ($\tau_{o\ max}$), modeling has been done varying the height of the slope from 5 to 30 m, the inclination from 10 to 30° and K_{oi} from 0.5 to 1.5. The results are shown on Figure 11a, where the maximum shear stress along the potential failure surface ($\tau_{o\ max}$) is plotted as a function of the slope height for different inclination and K_{oi} values. It can be seen that, for a slope inclined at 20° and having a K_{oi} of 0.5, the maximum shear stress along the potential failure surface varies from 11 to 67 kPa when the slope height increases from 5 to 30 m (Figure 11a). Similarly, for a slope having a height of 20 m and a K_{oi} of 0.5, a variation from 10 to 30° of the inclination increases the maximum shear stress along the potential failure surface ($\tau_{o\ max}$) from 28 to 56 kPa. In addition, varying K_{oi} from 0.5 to 1.5 for a slope having a height of 20 m and inclined at 20° to the horizontal, increases the maximum shear stress ($\tau_{o\ max}$) along the potential failure surface from 44 to 58 kPa. The increase of maximum shear stress ($\tau_{o\ max}$) with slope height and slope inclination can therefore be observed in this analysis. Moreover, the influence of K_{oi} on $\tau_{o\ max}$ seems to increase with slope height.

The maximum shear stress along the potential failure surface normalised to the soil unit weight and the slope height ($\tau_{o\ max}$ / ρgH) is plotted as function of the slope angle for different K_{oi} values and slope heights on Figure 11b. It can be seen that $\tau_{o\ max}$ / ρgH increases with slope angle and K_{oi} as well. Although the values are scattered, probably due to the influence of the height of the slope, the influence of the K_{oi} seems slightly larger for steeper slopes. Detailed description of the effect of geometry of the slope and K_{oi} on the initial stresses in a slope is given by Locat (2012).

4. Initiation and extent of progressive failure

The stresses in slopes generated by valley formation and their controlling parameters have been described in the above section. Using these stresses, a progressive failure analysis can be done with the method described in Section 2.4. In all cases, it is supposed that the failure is initiated along the potential failure surface where the shear stress is maximal ($\tau_{o\ max}$) and closer to the peak shear strength of the soil (point *A* on Figure 2b for example). The disturbing force (N_{ext}, see section 2.4.3) initiating progressive failure is therefore applied at this point in all cases.

This section presents the effect of the initial geometry and K_{oi} of a slope and the influence of the soil behaviour of the shear zone and soil layer above it on the critical change of stress initiating progressive failure ($\Delta\sigma_{crU}$) and the final extent of the progressive failure.

4.1. Effect of stresses in the slope

In Section 3, it was shown that high inclined slopes with large K_{oi} have high shear stress along a horizontal plane at the toe of the slope elevation. The effect of slope inclination on progressive failure initiation and propagation is presented in Figure 12 for slopes having a height of 20 m and inclination of 10 (Figures 12a,b and c), 20 (Figures 12d, e and f) and 30° (Figures 12g, h and i). It is observed that the critical unloading initiating progressive failure ($\Delta\sigma_{crU}$) equals 61, 55 and 50 kPa for slope angles of 10, 20 and 30° respectively (Figures 12c, f and i). Steeper slopes have higher initial shear stresses closer to the peak shear strength of the soil, which results in smaller $\Delta\sigma_{crU}$ values required to initiate progressive failure. It is also seen that the retrogression distance (L_R defined on Figure 2g) is 22, 45 and 71 m for slope angles of 10, 20 and 30° respectively (Figures 12b, e and h). The failure therefore propagates over larger distances when steeper slopes are considered.

Figure 13 shows the effect of K_{oi} on the initiation and the propagation of progressive failure for a slope having a height of 20 m and an inclination of 20°. Although the strength of the soil is influenced by K_o, it has been kept constant in this analysis to isolate the effect of K_{oi} on progressive failure. It can be seen that $\Delta\sigma_{crU}$ equals 55, 45 and 32 kPa for K_{oi} values of 0.5, 1.0 and 1.5 respectively (Figures 13c, e and g). The propagation of the failure surface is also affected by K_{oi}; K_{oi} values of 0.5, 1.0 and 1.5 give failure retrogressions (L_R) of 45, 103 and 155 m beyond the crest of the slope, respectively (Figures 13b, d and f). This is explained by the high shear stresses induced further inside the deposit when large K_{oi} values are considered.

Figure 14a shows the effect of the slope angle on $\Delta\sigma_{crU}$ for different K_{oi} on a slope having a height of 20 m. It can be observed that $\Delta\sigma_{crU}$ is essentially independent of Koi for a slope angle of 10° and then decreases with increasing slope angles and K_{oi} as explain above.

As presented in Section 3, the shear stress in a slope is larger for high slopes having high inclinations and high K_{oi}. In these cases, the maximum shear stress ($\tau_{o\ max}$) is closer to the peak shear strength of the soil, which explains the decrease of the perturbation $\Delta\sigma_{crU}$ necessary for initiating progressive failure in these conditions (Figure 12, 13 and 14a).

Figure 14b shows the effect of slope angle on the retrogression distance (L_R) for different K_{oi} values on slope having a height of 20 m. It is sown that L_R increases with increasing slope inclination and K_{oi}, except for Koi equal to 1.5, for which the retrogression distance seems to be approximately constant regardless of slope inclination. This indicates that, for very large K_{oi} values, failure progresses to a distance away from the toe of the slope, where slope angle has negligible influence.

As failure progresses further inside the deposit, the horizontal stress above the failure surface decreases and may fall below the undrained active failure criteria over a given length along the failure surface. The average undrained active strength (σ_{Act}) of the soil can be calculated with the following equation:

[14] $\sigma_{Act} = \frac{\gamma H}{2} - 2S_U$ (Lambe and Whitman 1969)

For a slope having a height (H) of 20 m, a total unit weight (γ) of 17 kN/m^3 and an average undrained strength (S_U) of 35 kPa, the average undrained active strength of the soil is:

[15] $\sigma_{Act} = \left(\frac{17\ \text{kN/m}^3 \times 20\ \text{m}}{2}\right) - (2\times 35\ \text{kPa}) = 100\ \text{kPa}$

For soil having larger OCR value (and larger K_o), the undrained strength will increase, giving lower undrained active strength. For example, for K_{oi} of 0.5, 1.0 and 1.5, the S_U of the soil may be 35 kPa, 60 and 80 kPa respectively, giving σ_{Act} values of 100, 50 and 10 kPa respectively. Figures 13c, e and g show the undrained active strength (σ_{Act}) from the left boundary to the crest of the slope, where the ground surface is horizontal. If the average horizontal stress falls below σ_{Act} (gray area on Figure 13c, e and g), active failure occur in the soil mass above the shear zone. It can be seen that, for the example presented in Figure 13, in cases where the soil has a high K_{oi} and high OCR values, the decrease in total stress during progressive failure might not be sufficient to cause active failure (average horizontal stress above active failure criteria, see Figure 13g). In these cases, the failure may propagate into the deposit without any active failure of the soil mass and no global failure of the slope occurs.

4.2. Influence of soil behaviour

Now that the effect of the stresses inside the slope has been illustrated, the influence of the soil stress-strain behaviour characteristics will be presented. First, the influence of the peak and large-deformation shear strengths of the soil in the shear zone will be examined. The displacements, at which these strengths are mobilised, will also be included in the study of the effect of stiffness and brittleness of the shear zone. Finally, the influence of the stiffness of the soil layer above the shear zone will be considered.

4.2.1. Influence of the peak and large-deformation shear strengths of the shear zone

As seen in the previous section, the larger the difference between the peak shear strength of the soil and the initial shear stress, the larger is the unloading needed to initiate progressive failure. For a given geometry and K_{oi}, high peak shear strength improves the stability regarding progressive failure by increasing the unloading necessary to initiate progressive failure. As this influence of the peak shear strength is quite straight forward, this study focuses on the influence of the post peak behaviour of the shear zone.

As explained in the introduction, progressive failure may be initiated in soils showing a strain-softening behaviour ($\tau_{ld} < \tau_p$, strain-softening behaviour). The influence of the large-deformation strength has been studied for a 20 m high slope inclined at 20° to the horizontal with a K_{oi} of 0.5 and a peak shear strength of 70 kPa by varying the large deformation shear strength. The displacements when these strengths are reached (δ_p and δ_{ld}) have been adjusted in order to keep the decrease in strength after the peak shear strength with the same slope. It has been seen by Locat (2012) that the unloading initiating progressive failure is not significantly influenced by the large-deformation shear strength. On the other hand, the retrogression of the failure (L_R) varies from 21 to 365 m when the large-deformation shear strength varies from 15 to 2 kPa, respectively, and tends towards 0 m for large-deformation shear strength larger than 18.2 kPa (Figures 15). This means that, for the case studied here, the large-deformation shear strength has to be lower than 18.2 kPa (Sensitivity larger than 3.8, given an intact shear strength of 70 kPa) in order for the loss of strength to be large enough to generate progressive failure. This indicates that τ_{ld} and thus sensitivity influences the propagation distance but not the susceptibility to progressive failure ($\Delta\sigma_{crU}$) and that for very small large-deformation shear strengths, the failure may retrogress over a very large distance.

4.2.2. Influence of the stiffness and the brittleness of the shear zone

Now that the effect of strength and sensitivity of the soil has been examined, it is necessary to look at the effect of stiffness. The behaviour of the shear zone before the peak shear strength can be studied by varying the stiffness of the shear zone and the post peak behaviour can be studied by varying the brittleness of the shear zone.

To quantify the brittleness of a soil, Bishop (1967 and 1971) introduced the brittleness index (I_B):

[16] $I_B = \frac{\tau_p - \tau_{ld}}{\tau_p} \times 100$

This index defines the percentage of reduction in shear strength when passing from the peak to the large-deformation shear strength. The higher I_B, the larger is the loss of strength from the peak shear strength to the large-deformation strength. It fails however to take into account the development of strain during softening.

In order to characterise the loss of shear strength with strain, D'Elia et al. (1998) suggested the general brittleness index (I_{GB}):

[17] $I_{GB} = \frac{\tau_p - \tau_{mob}}{\tau_p}$

This index uses the mobilised shear stress along the shear zone (τ_{mob}) which is function of shear strain. It varies from 0 at the peak to I_B when the soil reaches its large-deformation value, and specifies the variation of shear strength as strain develops.

Following this idea, it is possible to define a hardening (K_H) and a softening (K_S) parameters (linked to soil moduli and the thickness of the shear zone as indicated in Figures 8 and 9) taking into account the variation in shear strength of the soil with strain and using the horizontal displacement at the top of the shear zone during shear prior and after the peak shear strength. The stiffness and brittleness of the shear zone are therefore not just a function of the peak and large-deformation shear strengths of the soil (τ_p and τ_{ld}), but also a function of the displacements at the top of the shear zone at which the peak and large-deformation strengths are reached for an given shear zone thickness (δ_p and δ_{ld}, Figure 8). These parameters can then be defined with the following equations (Figure 9b):

[18] $K_H = \frac{\tau_p - \tau_o}{\delta_p}$

[19] $K_S = \frac{\tau_p - \tau_{ld}}{\delta_{ld} - \delta_p}$

K_H quantifies the gain in strength from the initial state of shear stress present along the shear zone (τ_o) up to the peak shear strength. High K_H values mean less deformation to reach the peak shear strength and high stiffness of the shear zone. K_S quantifies the rate of loss of strength from the peak shear strength down to the large-deformation shear strength. High K_S values mean small deformation to go from the peak shear strength down to the large-deformation shear strength and high brittleness. Therefore, two different shear zones having the same peak and large-deformation shear strengths (similar I_B) can therefore exhibit different stiffness (K_H) and brittleness (K_S) if these strengths are mobilised at different strains. K_H and K_S enable to quantify the stiffness and the brittleness of the shear zone which are related to the stress-strain characteristics of the soil, the shear stress before failure and the thickness of the shear zone (see Equations 9, 10, 18 and 19).

The effect of varying the brittleness of the shear zone is examined using shear strains at large deformation of 12.5 to 52%, corresponding to shear displacements to reach the large deformation of 0.0625 to 0.26 m respectively for a shear zone thickness of 0.5 m (see Equations 9 and 10). A 20 m high slope, inclined at 20 ° and K_{oi} of 0.5 with peak and remoulded shear strengths of 70 and 10 kPa is considered. This gives K_S values of 1043 to 235 kPa/m. In addition, the stiffness of the shear zone was studied with the variation of K_H obtained by using shear strain at the peak shear strength of 0.1% (t = 0.5 m, δ_p = 0.0005 m) and 10% (t = 0.5 m, δ_p = 0.05 m). This gives K_H values of 52245 and 522 kPa/m respectively. Sensitive clays should exhibits γ_p closer to 1% according to Leroueil et al. (1983). Extreme values of γ_p used in this study have been chosen to observe the effect of this parameter over a large range. Figure 16a presents the critical unloading initiating progressive failure as a function of K_S for both K_H values mentioned earlier. The resulting $\Delta\sigma_{crU}$ vary from 96 to 35 kPa for K_S varying from 235 to 1043 kPa/m respectively. It can be observed that $\Delta\sigma_{crU}$ decreases with increasing K_H and increasing K_S as well. However, K_H has a smaller influence than K_S on $\Delta\sigma_{crU}$. Figure 16b presents the relationship between the retrogression distance (L_R) and K_S for the same K_H values. It can be observed that, for a 20 m high slope, inclined at 20 ° and K_{oi} of 0.5, failure will propagate over a larger distance in brittle soil, with larger K_H and K_S values. K_H has also a smaller influence on the retrogression distance than K_S. In addition, Figures 16a and b show that soils with K_S value larger than 220 kPa/m are not brittle enough for progressive failure to be initiated and to propagate over a large distance.

These results indicate that slopes made of highly brittle soils are more susceptible to develop progressive failure (lower $\Delta\sigma_{crU}$) over a large distance (higher L_R). Such an influence of K_S on progressive failure was foreseen by D'Elia et al. (1998) but not proven numerically.

When soil has a high brittleness, smaller displacement is needed to induce the change in shear stress initiating progressive failure; as a result and according to Equation 2, $\Delta\sigma_{crU}$ is lower. In addition, when the failure propagates it progresses further into the deposit. This confirms that brittle soils are less stable, as a small unloading near the toe of the slope is needed to initiate a progressive failure and that failure will propagate over a larger distance.

4.2.3. Influence of the stiffness of the soil above the shear zone

In the progressive failure analysis used in this study, the soil above the shear zone expands horizontally, as a spring, and the average horizontal stress above the shear zone decreases according to the change of shear stress and the displacement in the shear zone. The influence of the stiffness of the upper soil layer (E_{el}) has been studied on a slope inclined at 20°, having a height of 20 m and a K_{oi} equal to 0.5. The behaviour of the shear zone is kept constant with peak and large-deformation shear strengths assumed to be 70 and 10 kPa respectively.

Figure 17 shows the effect of the stiffness (E_{el}) of the soil above the potential failure surface on the initiation and the extent of progressive failure. For stiffness varying from 5250 to 21000 kPa, $\Delta\sigma_{crU}$ from 34 to 94 kPa have been calculated respectively (Figures 17a). The calculated retrogression distance (L_R) of the failure after initiation decreases from 63 to 23 m for the above stiffness variation (Figure 17b). Therefore, soils with high stiffness need larger unloading for progressive failure to be initiated ($\Delta\sigma_{crU}$) and the failure, once initiated, propagates over a smaller distance inside the slope.

5. Discussion

The numerical method presented herein enables the consideration of the initial stresses in the slope before failure, using conventional finite element method, and the modeling of failure initiated near the toe of a slope and its propagation in space inside the deposit. It enables to study the main factors influencing the development of progressive failure and spreads in sensitive clays. However, many assumptions have been needed.

The result depends strongly on the initial shear stress along the potential failure surface (section 4.1). The initial shear stress calculated in PLAXIS is partly controlled by the state of stress prior valley formation, which is characterised by the K_o value of the deposit, and by the geometry of the slope. In addition, the soil model and its parameters influence the results from the numerical calculations. Furthermore, as explained in Section 2.3, the shear stress has been calculated by a one-step drained unloading to simulate valley formation. The unloading of the river valley in several different steps might influence the results. In order to validate the initial shear stress used in this study as a basis for progressive failure, study of the state of stress and deformation of clay slopes could be carried out.

Another factor influencing progressive failure is the strain-softening behaviour considered for the shear zone. The model in this study uses a stress-displacement relationship to model the horizontal displacement at the top of the shear zone and assumptions had to be made regarding the strain distribution in the shear zone, the shear zone thickness (*t*) and its evolution during shear (strain localisation was not considered in this analysis). The stress-displacement behaviour is input to interface elements representing the interface at the top of the shear zone. The shear zone thickness is therefore taken into account directly in the interface elements' soil model and does not depend on element size. However, the size of elements forming the mesh needs to be adjusted in order for the peak shear strength to be fully mobilised at a node of an interface element. This method enables to avoid mesh dependency problems but necessitate the latter assumptions.

As the movement along the shear zone is horizontal and the shear strain limited to the shear zone, the direct simple shear seems to be the most appropriate type of shearing to represent the shear zone behaviour forming the failure surface in spreads. Therefore, direct simple shear tests results can be used as input in the numerical model for the behaviour of the shear zone. However, the thickness of the shear zone and its evolution during shear during an actual spread are not straight forward notions to assess. The analysis presented herein evidences the need of a better understanding of clay response when subjected to shear in order to understand failure initiation and propagation and to input more representative soil model in the numerical analysis. In particular, work is needed in the determination of the post-peak shear behaviour, shear zone thickness, and shear strain localisation. This would help defining appropriate K_H and K_S values to input in the model.

The results of this study corroborate well results from other studies brought out in the introduction (Lo and Lee 1973*a* and *b*; Quinn et al. 2011 and 2012; Gylland et al. 2010) and show the importance of the brittleness of the soil and the large-deformation shear strength on progressive failure. Even with the limitations mentioned in the previous paragraphs, the method enables to numerically confirm the effect of the geometry and soil behaviour on upward progressive failure that may explain spreads in sensitive clays. The interests of the presented numerical method and its improvements regarding previous models are:

- The initial stresses in a slope induced by valley formation are taken into account in the analysis with a conventional finite element model;

- The modeling of the failure propagation in space considers a strain-softening behaviour for the shear zone enabling the study of progressive failure as described by Bernander (2000, 2008 and 2011), Locat et al. (2011) and Locat (2012);
- The study gives a mechanical and numerical explanation of the failure initiation by a critical unloading near the toe of the slope and its propagation inside the deposit which might explains spreads occurring in sensitive clays;
- The analysis is done using conventional numerical tools and geotechnical properties of the soil.

It can be noted that slopes and clays in which spreads have been observed seem to present the characteristics necessary for progressive failure initiation and propagation. They are:

- Cases of spreads have been reported to occur in lightly overconsolidated soil (the 1988 Brownsburg spread for example, see Fortin-Rhéaume 2013), Eastern Canadian clays are generally overconsolidated ($1.2 < OCR < 2.5$, from Leroueil et al. 1983), which can contribute to progressive failure initiation and mainly to high propagation distances (Figures 13 and 15).
- Eastern Canadian clays may exhibit peak shear strengths generally mobilised at strains ranging from 0.3 to 1.2% and brittle stress-strain behaviour (Leroueil et al. 1983), which could indicate that a small disturbance is needed to initiate the movement and failure can propagate over large distance (Figure 16).
- Low remoulded shear strengths, such as those observed in Eastern Canadian clays that are often below 1.5 kPa indicate low large-deformation shear strength and may explain the large failure surface extents (Figures 15) observed in spreads.

6. Conclusion

This paper presents a study of the factors influencing the initiation and propagation of upward progressive failure initiated near the toe of sensitive clay slopes formed by valley formation. The study was done using PLAXIS 2D 2010 (PLAXIS Manuals 2011) to evaluate the shear stress in the slope before failure and BIFURC (Jostad and Andresen 2002) to model the initiation and propagation of the failure using the shear stress calculated in PLAXIS and a strain-softening behaviour. The analysis focuses on the factors influencing the initial stresses in the slope and the mechanical behaviour of the shear zone. It is shown that:

- Shear stress along a horizontal plane at the elevation of the toe of the slope is larger and closer to the peak shear strength of the soil (τ_p) when high, steep slopes with large K_{oi} are considered. Therefore, high, steep slopes having large K_{oi} are more susceptible to progressive failure initiation, smaller disturbance being needed to initiate failure, and the failure propagates over a larger distance.
- All other parameters considered being the same, lower large-deformation shear strength (τ_{ld}), or larger sensitivity, leads to larger propagation distances.
- Soils having a brittle behaviour, defined as a rapid decrease of strength beyond the peak shear strength (τ_p) or larger K_S value for the shear zone (Equation 19), are more susceptible to progressive failure, as less unloading is needed to initiate the failure which propagates over a larger distance inside the deposit.
- Less unloading is needed to initiate failure in soil having low stiffness (E_{el}) and if initiated, the failure propagates over a larger distance.

The results obtained from this analysis generally corroborate previous numerical studies of progressive failure made in the context of long landslides in gently inclined sensitive clay slopes (Bernander 2000, 2008 and 2011, Bernander and Olofsson 1981*a* and *b*, Gylland and Jostad 2010 and Gylland et al.

2010) and in the context of delayed failures initiated near the toe of clay slopes (Kovacevic et al. 2004 and 2007 and Lo and Lee 1973*a* and *b*). Similarly to Quinn et al. (2011 and 2012), this study concludes that sensitive clays from Eastern Canada may be susceptible to progressive failure initiation. Progressive failure can therefore be initiated in these clays, decrease the horizontal stress, causing active failure of an extensive part of the slope and may lead to a spread. Moreover, the high sensitivity and the low remoulded shear strength of these clays explain the large retrogression distances observed in some spreads.

The progressive failure mechanism presented in this study is a simplified version of progressive failure explaining spreads in sensitive clays. In reality the problem is influenced by strain-rate effects and geometric changes of the failing soil mass. In addition, the shear strains in the entire soil mass before shear localisation and formation of the failure surface affect the results of the analysis and add uncertainty to the results. The attention has also been given to the propagation and the extent of the shear zone in which the failure surface is formed. In order to completely understand the mechanism forming spreads, attention should also be given to the dislocation of the soil mass when active failure of the slope occurs and the formation of horsts and grabens. In order to do that, two dimensional numerical methods would have to be used to study the failure mechanism as Andresen and Jostad (2004 and 2007) and Hanssen and al. (2011) did for translational progressive landslides. Furthermore, the model presented herein used unloading by a first slide or rapid erosion as initiation for the progressive failure. The effect of gradual small erosion on a slope and high hydraulic gradient at the toe of a slope should also be studied as triggering mechanisms for progressive failure in relation to spreads. At last, the model must be tested on well documented cases of spreads occurring in sensitive clays.

7. Acknowledgments

The authors would like to acknowledge the financial contributions of the The Natural Sciences and Engineering Research Council of Canada and the Fonds québécois de recherche sur la nature et les technologies. The authors are also grateful to the Norwegian Geotechnical Institute for the technical and financial support they provided. The authors would also like to thank Dr. P. Quinn and two other anonymous reviewers for their critical reviews that improved the quality of this paper.

8. References

Andresen, L. and Jostad, H. P. 2004. Analyses of progressive failure in long natural slopes. In Proceeding of the 9th Symposium on Numerical Models in Geomechanics - NUMOG IX, Ottawa, Canada, Ont. A.A. Balkema, Leiden, the Netherlands, pp. 603-608.

Andresen, L. and Jostad, H. P. 2007. Numerical modeling of failure mechanisms in sensitive soft clay - Application to offshore geohazards. In Proceedings of the Offshore Technology Conference 2007, Houston, Texas, May 2007. Offshore Technology Conference, Richardson, Texas. Paper OTC 18640.

Bernander, S. 2000. Progressive landslides in long natural slopes, formation, potential extension and configuration of finished slides in strain-softening soils. Licentiate Thesis, Department of Civil and Mining Engineering, Luleå University of Technology, Luleå, Sweden.

Bernander, S. 2008. Down-hill progressive landslides in soft clays, triggering disturbance agents, slide propagation over horizontal or gently sloping ground, sensitivity related to geometry. Department of Civil and Mining Engineering, Luleå University of Technology, Luleå, Sweden. Research Report.

Bernander, S. 2011. Progressive Landslides in Long Natural Slopes, Formation, Potential Extention and Configuration of Finished Slides in Strain-Softening Soils. Licentiate Thesis, Department of Civil and Mining Engineering, Luleå University of Technology, Luleå, Sweden.

Bernander, S. and Olofsson, I. 1981*a*. On formation of progressive failure in slopes. In Proceedings of the 10th International Conference on Soil Mechanics and Foundation Engineering (ICSMFE), Stockholm, Sweden, A.A. Balkema, Rotterdan, the Netherlands. pp. 357-362.

Bernander, S. and Olofsson, I. 1981*b*. The landslide at Tuve in November 1977. Department of Civil and Mining Engineering, Luleå University of Technology, Luleå, Sweden. Technical Report.

Bishop, A. W. 1967. Progressive failure - with special reference to the mechanism causing it. In Proceedings of the Geotechnical Conference, Oslo, Norway. Norwegian Geotechnical Institute, Oslo, Norway. Volume 2, pp. 142-150.

Bishop, A. W. 1971. The influence of progressive failure on the choice of the method of stability analysis. Géotechnique, **21**: 168-172.

Bjerrum, L. 1967. Progressive failure in slopes in overconsolidated plastic clay and clay shales. Terzaghi Lecture, Journal of Soil Mechanics and Foundations Division, ASCE. **93**(5): 3-49.

Carson, M.A. 1977. On the retrogression of landslides in sensitive muddy sediments. Canadian Geotechnical Journal, **14**(4): 582-602.

Carson, M. A. 1979a. Le glissement de Rigaud (Québec) du 3 Mai 1978: Une interprétation du mode de rupture d’après la morphologie de la cicatrice. Géographie physique et Quaternaire, **33**(1): 63-92.

Carson, M.A. 1979b. On the retrogression of landslides in sensitive muddy sediments: Reply. Canadian Geotechnical Journal, **16**(2): 431-444.

Christian, J. T. and Whitman, R. V. 1969. A one-dimensional model for progressive failure. In Proceedings of the 7th International Conference of Soil Mechanic and Foundation Engineering, Mexico City, Mexico. Societad Mexicana de Mecànica de Suelos, A. C. Volume 2, pp. 541-545.

Cruden, D. M. and Varnes D. J. 1996. Landslides types and processes. In Landslides investigation and mitigation, Special Report 247, Transportation, Research Board, National Research Council, Edited by A. K. Turner, and R. L. Schuster, National Academy press, Washington, D.C. pp. 37-75.

Demers, D., Robitaille, D., Locat, P., and Potvin, J., 2013. Inventory of large landslides in sensitive clay in the province of Quebec, Canada : Preliminary analysis. In Proceedings of the 1st International Workshop on Landslides in Sensitive Clays, Landslides in sensitive clays – From geosciences to risk management, Québec, Qc. October 28-30 2013. *In press*.

D'Elia, B., Picarelli, L., Leroueil, S. and Vaunat, J. 1998. Geotechnical characterisation of slope movements in structurally complex clay-soils and stiff jointed clays. Italian Geotechnical Journal, **32** (3) : 5-32.

Fortin-Rhéaume, A.-A. 2013. Étude de l'étalement latéral de 1988 et des autres glissements de terrain le long de la vallée à Brownsburg-Chatham, Québec. M.Sc. Thesis, Département de génie civil, Université Laval, Québec, Qc.

Grondin, G. and Demers, D. 1996. The Saint-Liguori flakeslide: Characterisation and remedial works. In Proceedings of the 7th International Symposium on Landslides, Trondheim, Norway. Edited by K. Senneset. Balkema, Rotterdam, the Netherlands. Volume 2, pp. 743-748.

Gylland, A. S. and Jostad, H. P. 2010. Effect of updated geometry in analyses of progressive failure. In Proceedings of the 7th European Conference on Numerical Method in Geotechnique, Trondheim, Norway. pp. 459-502.

Gylland, A. S., Sayd, M. S., Jostad, H. P. and Bernander S. 2010, Investigation of soil property sensitivity in progressive failure. In Proceedings of the 7th European Conference on Numerical Method in Geotechnique, Trondheim, Norway. pp. 515-520.

Hamouche, K. K., Leroueil, S., Roy, M. and Lutenegger, A. J. 1995, In situ evaluation of K_0 in eastern Canada clays, Canadian Geotechnical Journal, **32**(4): 677-688.

Hanssen, S. B., Gylland, A. S. and Nordal, S. 2011. Simulation of the Smaaroed Landslide in soft sensitive clay using a rate dependent, strain softening model. In Proceedings 13th International Conference of International Association for Computer Methods and Advances in Geomechics, Melbourne, Australia. pp. 1183-1189.

Jostad, H. P. and Andresen, L. 2002. Capacity analysis of anisotropic and strain-softening clays. In Proceedings of the NUMOG VIII. Rome, Italy. pp. 469-474.

Kovacevic, N., Hight, D. W. and Potts, D. M. 2004. Temporary slope stability in London clay - Back analyses of two case histories. In Advances in geotechnical engineering: The Skempton Conference, London. Thomas Telford Publishing, London. Volume 2, pp. 842-855.

Kovacevic, N., Hight, D. W. and Potts, D. M. 2007. Predicting the stand-up time of temporary London Clay slopes at Terminal 5, Heathrow Airport. Géotechnique, **57**(1): 63-74.

Lambe, T. W. and Whitman, R. V. 1969. Soil Mechanics. John Wiley and sons Inc. New-York 553p.

Leroueil, S. 2001. 39th Rankine Lecture: Natural slopes and cuts: movement and failure mechanisms. Géotechnique, **51**(3): 197-243.

Leroueil, S., Locat, A., Eberhardt, E. and Kovacevic, N. 2012. Keynote Lecture: Progressive failure in natural and engineering slopes, In Proceedings of the 11th International and 2nd North American Symposium on Landslides, 3-8 June, Banff, Alberta, pp. 31-46.

Leroueil, S., Tavenas, F. and Le Bihan J.-P. 1983. Propriétés caractéristiques des argiles de l'est du Canada. Canadian Geotechnical Journal, **20**(4): 681-705.

Lo, K. Y. 1972. An Approach to the Problem of Progressive Failure. Canadian Geotechnical Journal, **9**(4): 407-429.

Lo, K. Y. and Lee, C. F. 1973*a*. Stress analysis and slope stability in strain softening soils. Géotechnique, **23**(1): 1-11.

Lo, K. Y. and Lee, C. F. 1973*b*. Analysis of progressive failure in clay slopes. In Proceedings of the 8th International Conference on Soil Mechanic and Foundation Engineering, Moscow. ICSMFE Publications, USSR. Volume 1, pp. 251-258.

Locat, A. 2007. Étude d'un étalement latéral dans les argiles de l'Est du Canada et de la rupture progressive, Le cas du glissement de Saint-Barnabé-Nord. M.Sc. Thesis, Département de génie civil, Université Laval, Québec, Qc.

Locat, A. 2012. Rupture progressive et étalements dans les argiles sensibles. PhD. Thesis, Département de génie civil et de génie des eaux, Université Laval, Québec, Qc.

Locat, A., Leroueil, S., Bernander, S., Demers, D., Locat, J., Ouehb, L. 2008. Study of a lateral spread failure in an eastern Canada clay deposit in relation with progressive failure: The Saint-Barnabé-Nord Slide. In Proceedings of the 4th Canadian Conference on Geohazards: From Causes to Management. Québec, Que. Edited by J. Locat, D. Perret, D. Turmel, D. Demers et S. Leroueil, Presses de l'Université Laval, Québec, Que. pp. 89-96.

Locat, A., Leroueil, S., Bernander, S., Demers, D., Jostad, H. P. and Ouehb, L. 2011*a*. Progressive failures in Eastern Canadian and Scandinavian sensitive clays. Canadian Geotechnical Journal, **48**(11): 1696-1712.

Locat, P., Fournier, T., Robitaille, D. and Locat, A. 2011*b*. Glissement de terrain du 10 mai 2010 Sainte-Jude, Montérégie, rapport sur les caractéristiques et les causes. Raport, Ministère des Transports du Québec, Que.

Odenstad, S. 1951. The landslide at Sköttorp on the Lidan River, February 2, 1946. Royal Swedish Institute Proceedings, **4**: 1–38.

Ouehb, L. 2007. Analyse du glissement de Saint-Liguori (1989) dans l'optique d'une rupture progressive. M.Sc. Thesis, Departement de génie civil, Université Laval, Québec, Qc.

Palmer, A. C. and Rice, J. R. 1973. The growth of slip surfaces in the progressive failure of overconsolidated clay. In Proceedings of the Royal Society of London, Series A, Mathematical and Physical Sciences, **332**(1591): 527-548.

PLAXIS Manuals. 2011. PLAXIS 2D 2010. PLAXIS bv. Delft. Netherlands.

Quinn, P. E., Diederichs, M. S., Rowe, R. K. and Hutchinson, D. J. 2011. A new model for large landslides in sensitive clay using a fracture mechanism approach. Canadian Geotechnical Journal, **48**(8): 1151-1162.

Quinn, P. E., Diederichs, M. S., Rowe, R. K. and Hutchinson, D. J. 2012. Development of progressive failure in sensitive clay slopes. Canadian Geotechnical Journal, **49**: 782-795.

Skempton, A. W. 1964. 4th Rankine Lecture : Long-term stability of clay slopes. Géotechnique, **14**(2): 77-102.

Terzaghi, K. and Peck, R. B. 1948. Soil Mechanics in Engineering Practice. John Wiley and Sons, Inc., New-York.

Urciuoli, G., Picarelli, L. and Leroueil, S. 2007. Local soil failure before general soil failure. Geotechnical and Geological Engineering Journal, **25**(1): 103-122.

Table captions:

Table 1: Soil properties used in PLAXIS.

Table2: Soil properties used in BIFURC

Figure captions:

Figure 1: Illustration of spread with horsts and grabens.

Figure 2: Initial condition (time 0), initiation (time 1) and final extension (time 2) of upward progressive failure. (a) Geometry of the slope, potential failure surface (dashed line) and failure surface defined where the soil is beyond the peak shear strength (thick dotted line); (b, e, and g) shear stress acting along the potential failure surface; (c, f, and h) average total horizontal stress above the shear zone; and (d) stress-displacement behaviour of the shear zone. *A*, *a*, *b*, *a'* and *b'* are points along the x-axis where attention is drawn to (d, e, and g) the shear stress along the potential failure surface and (f and h) horizontal total stress in the soil mass above the potential failure surface.

Figure 3: Horizontal equilibrium acting on the soil mass above the potential failure surface; figure shows the change in average total horizontal stress ($\Delta\sigma_x$) over a height H_x, corresponding to a change in shear stress (τ_x - τ_o) over a length (L) along the potential shear zone.

Figure 4: Geometry, mesh and boundary conditions used in PLAXIS (a) before and (b) after valley formation.

Figure 5: Main characteristics of the Hardening Soil Model: (a) stress-strain behaviour during oedometer compression; (b) a hyperbolic deviatoric stress (q) vs. axial strain (ε_1) relationship during drained shear; and (c) cone hardening controlled by mobilised friction and pre-consolidation stress (p'_c) controlled cap hardening (modified from PLAXIS Manuals 2011).

Figure 6: Horizontal equilibrium of a vertical section between j and j-1 of the soil mass above the cross-section on Figure 4b; E_j and E_{j-i} are the horizontal forces due to earth pressure in the soil mass, H_j and H_{j-1} are the height of the soil mass above the cross-section and $\tau_{o\ average\ j}$ is the average shear stress along a length L_j of the potential failure surface corresponding to the change in horizontal force due to earth pressure ΔE_i.

Figure 7: Schematic representation of: (a) division of the soil mass; (b) element types; and (c) mesh and boundary conditions used in BIFURC.

Figure 8: (a) Stress-strain behaviour converted into a (b) stress-displacement behaviour.

Figure 9: (a) Stress-strain behaviour; and (b) stress-displacement behaviour used in this study for a shear zone thickness of 0.5 m with definitions of the soil parameters, including the hardening parameter K_H and softening parameter K_S (τ_o will vary along the potential failure surface as schematized on Figure 2b).

Figure 10: (a) Example of a load displacement curve obtained with BIFURC; and (b) propagation of shear stress along the potential failure surface for different increments. *A* is a point along the x-axis where attention is drawn to the shear stress along the potential failure surface.

Figure 11: Influence of (a) slope height on the maximum shear stress along the potential failure surface ($\tau_{o\ max}$), for slopes inclined at 10, 20 and 30° (different shades of grey area); and (b) influence of the slope angle on the normalised maximum shear stress ($\tau_{o\ max}$ / ρgH); shaded areas show K_{oi} values varying from 0.5 to 1.5 for different inclinations and different height.

Figure 12: Effect of slope inclination on progressive failure. Figures show: (a, d, g) the geometry; (b, e, h) the shear stress along the potential failure surface; and (c, f, i) the average horizontal total stress above the potential failure surface, before failure (time 0), for the initiation stage (time 1) and for the final stage (time 2). Undrained peak shear and large-deformation shear strengths (τ_p and τ_{ld}), critical unloading stress initiating progressive failure ($\Delta\sigma_{crU}$) and undrained active strength (σ_{Act}) are also indicated. Slopes having a height of 20 m and K_{oi} of 0.5 are considered.

Figure 13: Effect of K_{oi} on progressive failure. Figures show: (a) the geometry; (b, d, f) the shear stress along the potential failure surface; and (c, e, g) the average horizontal total stress above the potential failure surface, before failure (time 0), for the initiation stage (time 1) and for the final stage (time 2). Undrained peak shear and large-deformation shear strengths (τ_p and τ_{ld}), critical unloading stress initiating progressive failure ($\Delta\sigma_{crU}$) and undrained active strength (σ_{Act}) are also indicated. Slopes having a height of 20 m inclined at 20° are considered.

Figure 14: Influence of the slope angle on (a) the critical unloading stress initiating progressive failure ($\Delta\sigma_{crU}$) and (b) the retrogression distance (L_R) for different K_{oi} values. Slopes having a height of 20 m and peak and large deformation shear strengths of 70 and 10 kPa respectively are considered.

Figure 15: Retrogression distance (L_R) of the failure surface as a function of τ_{ld} for a slope inclined at 20° and having a height of 20 m, K_{oi} of 0.5 and a peak shear strength of 70 kPa.

Figure 16: Influence of K_S on (a) the critical unloading stress initiating progressive failure ($\Delta\sigma_{crU}$); and (b) the retrogression distance of the failure surface during progressive failure (L_R). Shaded areas show the effect of variation of K_H. Slopes having a height of 20 m, 20° of inclination and peak and large deformation shear strengths of 70 and 10 kPa respectively are considered.

Figure 17: Effect on E_{el} on the (a) the critical unloading stress initiating progressive failure ($\Delta\sigma_{crU}$); and (b) the retrogression distance of the failure surface during progressive failure (L_R). Slopes having a height of 20 m, 20° of inclination and peak and large deformation shear strengths of 70 and 10 kPa respectively are considered.

Table 1: Soil properties used in PLAXIS.

Parameter	Symbol	Value
Material Model	*Model*	Hardening Soil Model
Type of material behaviour	*Type*	Drained
Soil unit weight above w.t.	ρg	17 kN/m^3
Soil unit weight below w.t.	ρg	17 kN/m^3
Horizontal permeability	k_x	10^{-9} m/s
Vertical permeability	k_y	10^{-9} m/s
Reference secant Young modulus	E_{50}^{ref}	21000 kPa
Reference tangent oedometer modulus during virgin loading	E_{oed}^{ref}	21000 kPa
Reference unloading / reloading modulus	E_{ur}^{ref}	63000 kPa
Power for stress dependent stiffness	m	1
Reference stress	p_{ref}	100 kPa
Failure ratio	R_f	0.9
Poisson's ratio	ν'_{ur}	0.25
Lateral stress coefficient	K_o^{OC}	0.43
Cohesion	c'	35 kPa
Friction angle	ϕ'	35°
Dilatancy angle	ψ	0°

Table2: Soil properties used in BIFURC

Parameter	Symbol	Value
Truss elements		
Stiffness modulus[1]	E_{el}	10500 (5250 - 21000) kPa
Interface elements		
Peak shear strength	τ_p	70 kPa
Large-deformation shear strength[1]	τ_{ld}	10 (2 - 18.3) kPa
Peak shear strain[1]	γ_p	1 (0.1 - 10) %
Large-deformation shear strain[1, 2]	γ_{ld}	25 (12.5 - 52) %
Shear zone thickness	t	0.5 m
Displacement at the peak[1, 3]	δ_p	0.005 (0.0005 - 0.05) m
Large-deformation displacement[1, 2, 4]	δ_{ld}	0.125 (0.0625 - 0.26) m

[1] Values in parenthesis show range used in the parametric study.
[2] Strain or displacement at which the large-deformation shear strength is mobilized.
[3] Calculated with Equation 9
[4] Calculated with Equation 10

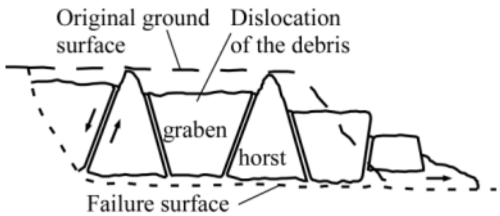

Figure 1: Illustration of spread with horsts and grabens.

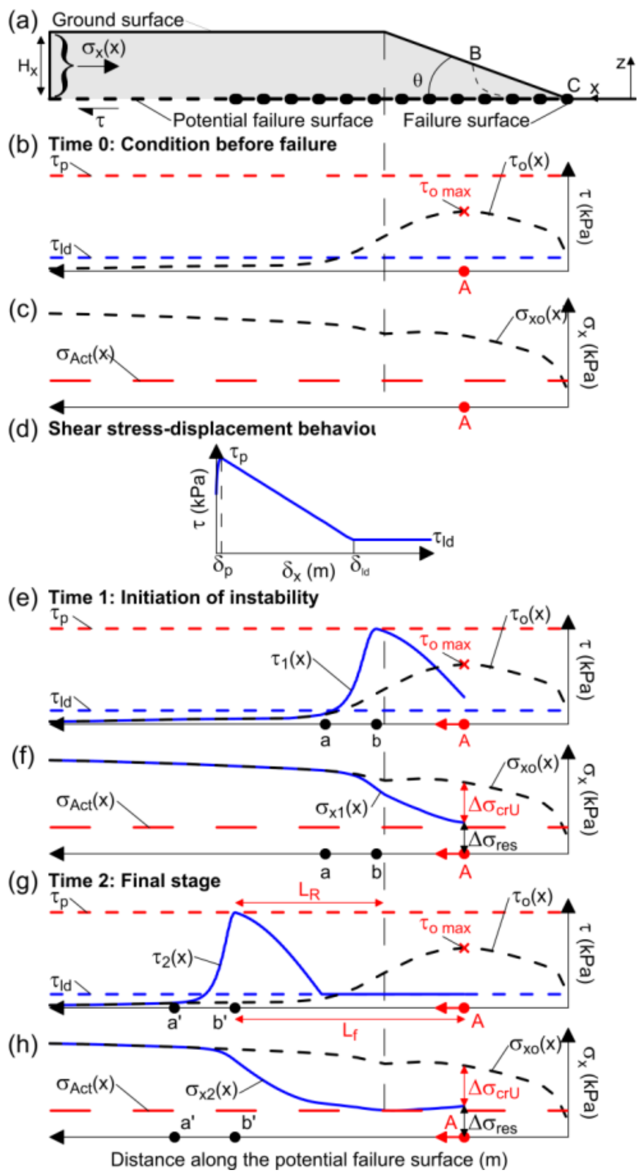

Figure 2: Initial condition (time 0), initiation (time 1) and final extension (time 2) of upward progressive failure. (a) Geometry of the slope, potential failure surface (dashed line) and failure surface defined where the soil is beyond the peak shear strength (thick dotted line); (b, e, and g) shear stress acting along the potential failure surface; (c, f, and h) average total horizontal stress above the shear zone; and (d) stress-displacement behaviour of the shear zone. *A*, *a*, *b*, *a'* and *b'* are points along the x-axis where attention is drawn to (d, e, and g) the shear stress along the potential failure surface and (f and h) horizontal total stress in the soil mass above the potential failure surface.

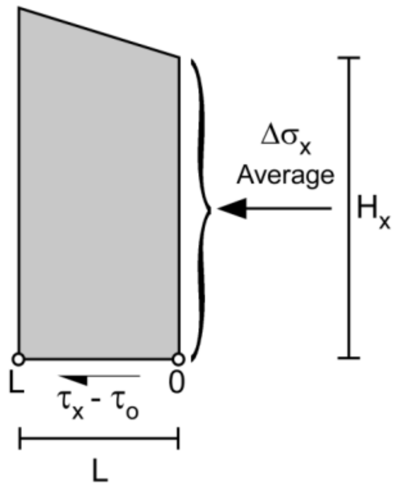

Figure 3: Horizontal equilibrium acting on the soil mass above the potential failure surface; figure shows the change in average total horizontal stress ($\Delta\sigma_x$) over a height H_x, corresponding to a change in shear stress (τ_x - τ_o) over a length (L) along the potential shear zone.

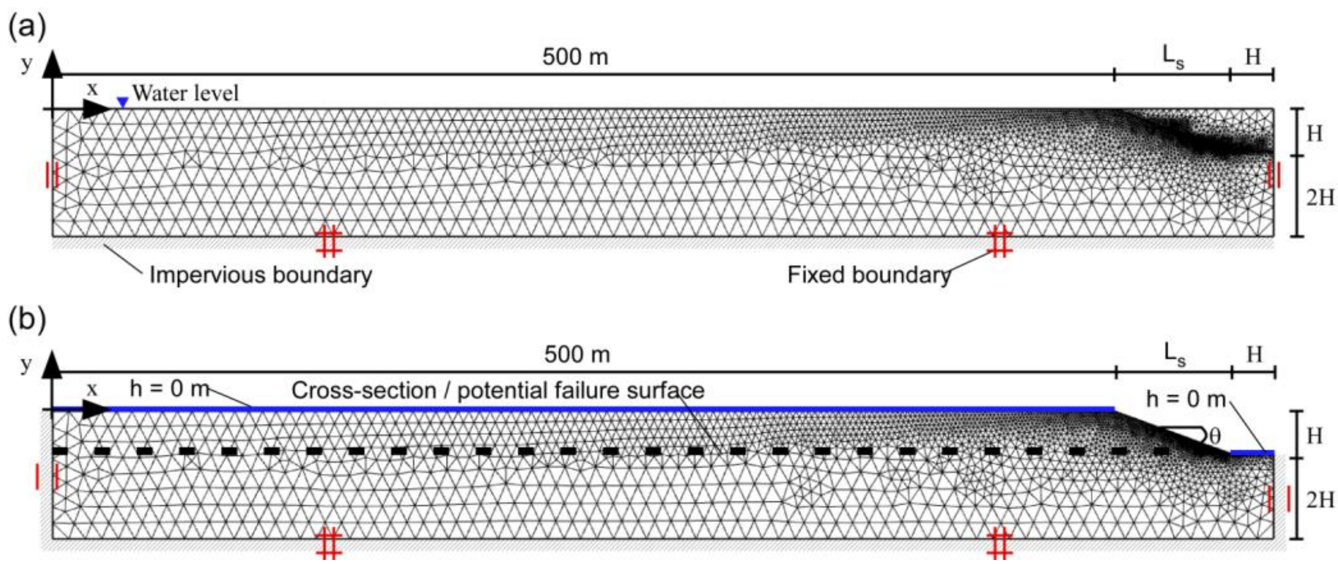

Figure 4: Geometry, mesh and boundary conditions used in PLAXIS (a) before and (b) after valley formation.

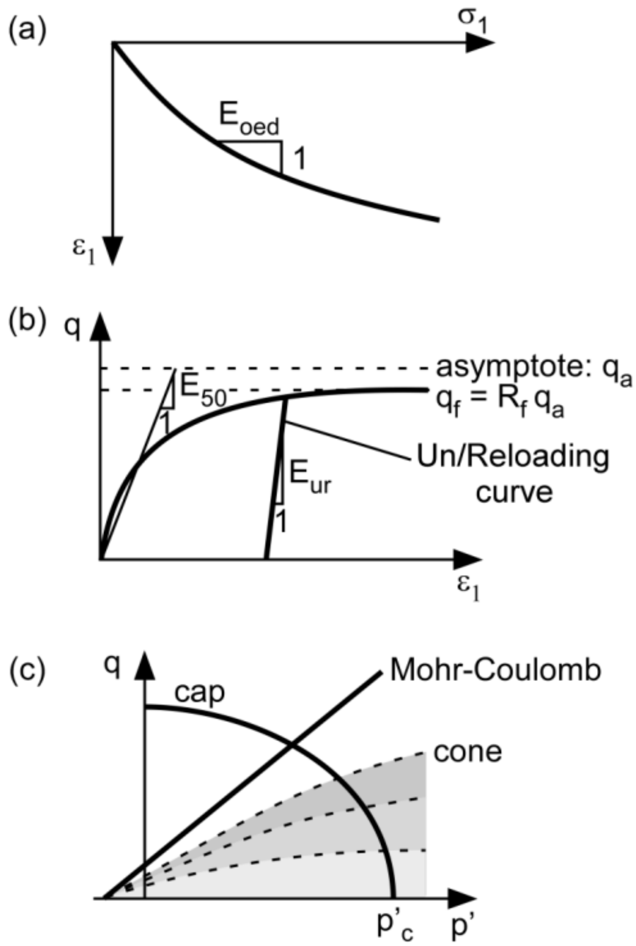

Figure 5: Main characteristics of the Hardening Soil Model: (a) stress-strain behaviour during oedometer compression; (b) a hyperbolic deviatoric stress (q) vs. axial strain (ε_1) relationship during drained shear; and (c) cone hardening controlled by mobilised friction and pre-consolidation stress (p'_c) controlled cap hardening (modified from PLAXIS Manuals 2011).

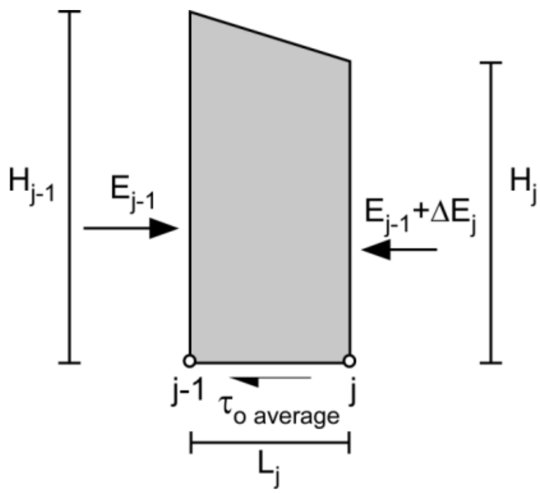

Figure 6: Horizontal equilibrium of a vertical section between j and j-1 of the soil mass above the cross-section on Figure 4b; E_j and E_{j-i} are the horizontal forces due to earth pressure in the soil mass, H_j and H_{j-1} are the height of the soil mass above the cross-section and $\tau_{o\ average\ j}$ is the average shear stress along a length L_j of the potential failure surface corresponding to the change in horizontal force due to earth pressure ΔE_i.

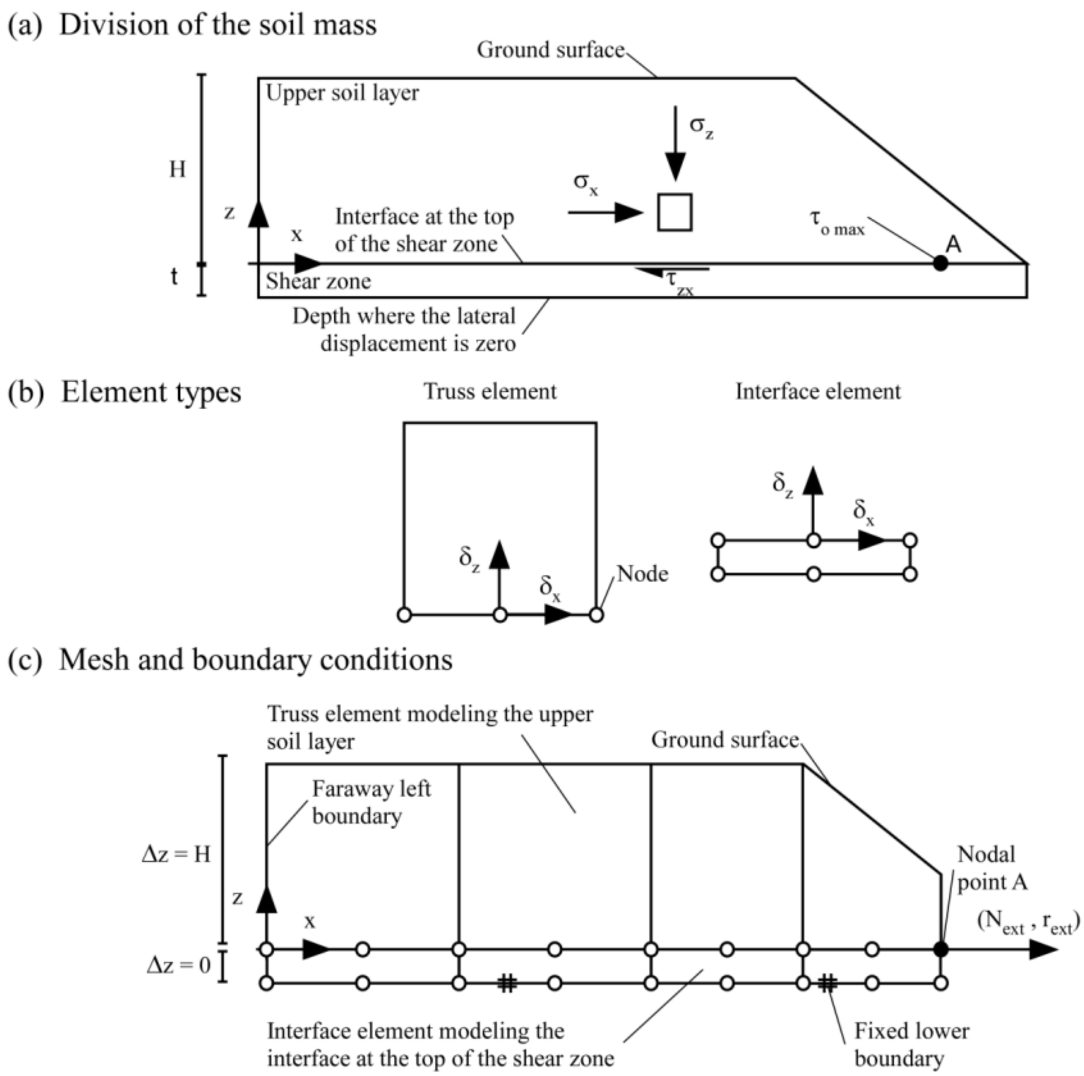

Figure 7: Schematic representation of: (a) division of the soil mass; (b) element types; and (c) mesh and boundary conditions used in BIFURC.

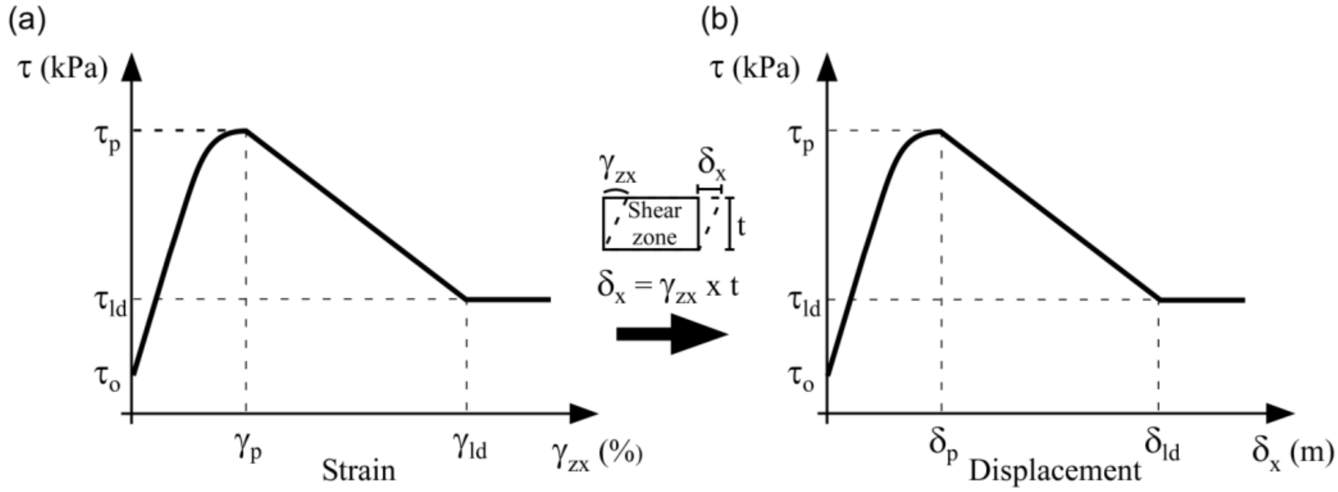

Figure 8: (a) Stress-strain behaviour converted into a (b) stress-displacement behaviour.

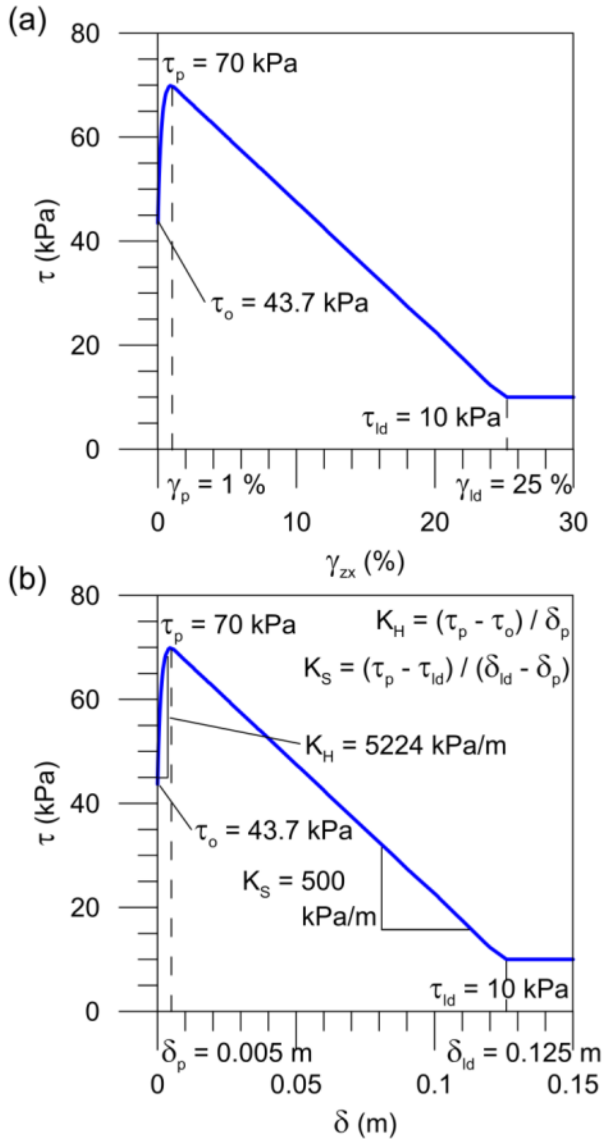

Figure 9: (a) Stress-strain behaviour; and (b) stress-displacement behaviour used in this study for a shear zone thickness of 0.5 m with definitions of the soil parameters, including the hardening parameter K_H and softening parameter K_S (τ_o will vary along the potential failure surface as schematized on Figure 2b).

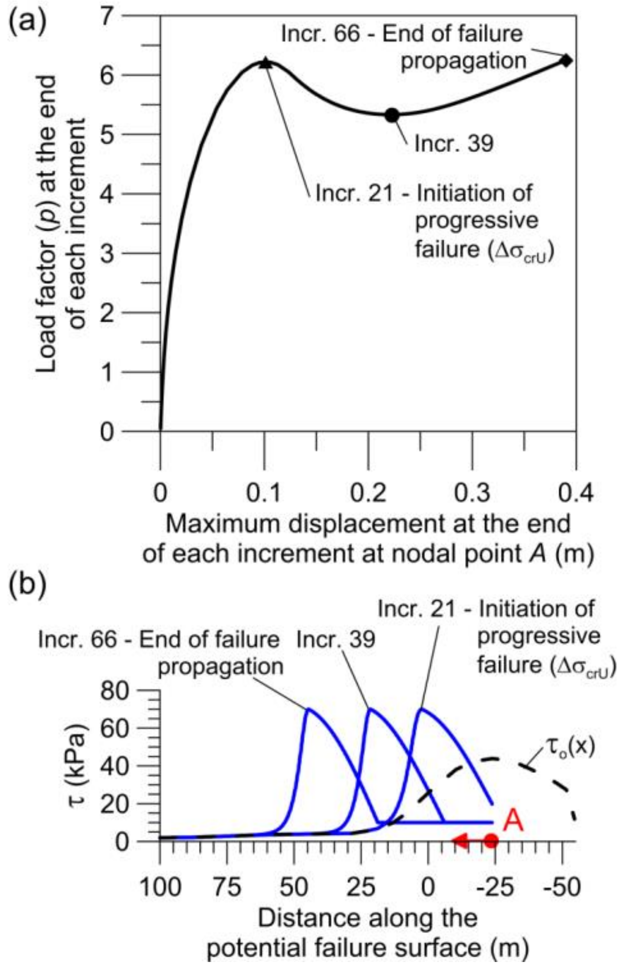

Figure 10: (a) Example of a load displacement curve obtained with BIFURC; and (b) propagation of shear stress along the potential failure surface for different increments. *A* is a point along the x-axis where attention is drawn to the shear stress along the potential failure surface.

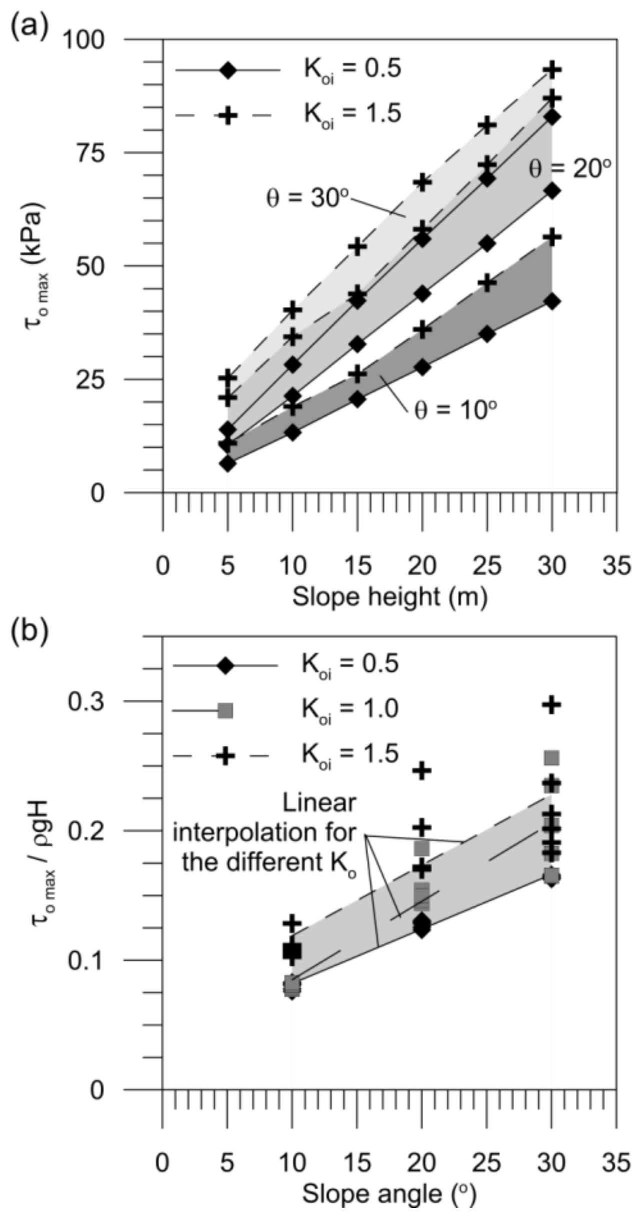

Figure 11: Influence of (a) slope height on the maximum shear stress along the potential failure surface ($\tau_{o\ max}$), for slopes inclined at 10, 20 and 30° (different shades of grey area); and (b) influence of the slope angle on the normalised maximum shear stress ($\tau_{o\ max}$ / ρgH); shaded areas show K_{oi} values varying from 0.5 to 1.5 for different inclinations and different height.

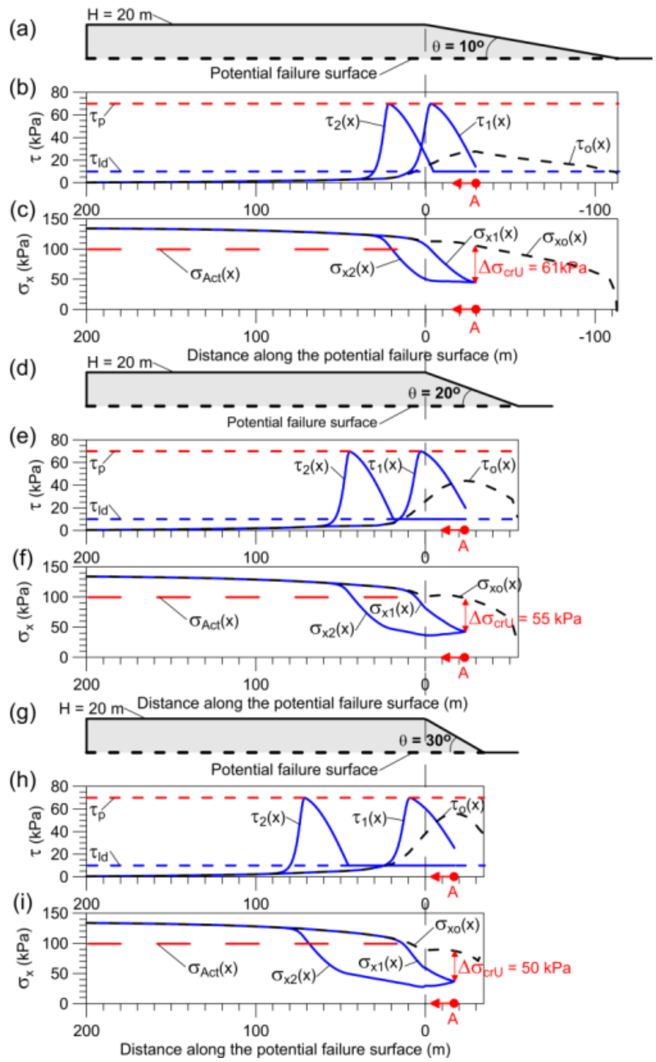

Figure 12: Effect of slope inclination on progressive failure. Figures show: (a, d, g) the geometry; (b, e, h) the shear stress along the potential failure surface; and (c, f, i) the average horizontal total stress above the potential failure surface, before failure (time 0), for the initiation stage (time 1) and for the final stage (time 2). Undrained peak shear and large-deformation shear strengths (τ_p and τ_{ld}), critical unloading stress initiating progressive failure ($\Delta\sigma_{crU}$) and undrained active strength (σ_{Act}) are also indicated. Slopes having a height of 20 m and K_{oi} of 0.5 are considered.

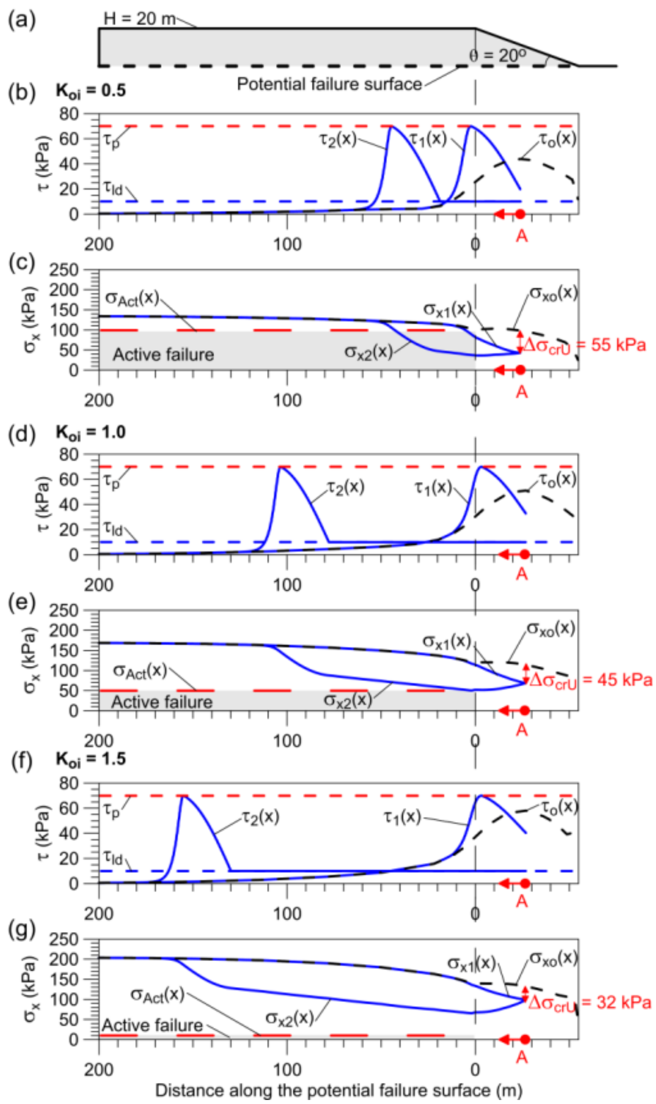

Figure 13: Effect of K_{oi} on progressive failure. Figures show: (a) the geometry; (b, d, f) the shear stress along the potential failure surface; and (c, e, g) the average horizontal total stress above the potential failure surface, before failure (time 0), for the initiation stage (time 1) and for the final stage (time 2). Undrained peak shear and large-deformation shear strengths (τ_p and τ_{ld}), critical unloading stress initiating progressive failure ($\Delta\sigma_{crU}$) and undrained active strength (σ_{Act}) are also indicated. Slopes having a height of 20 m inclined at 20° are considered.

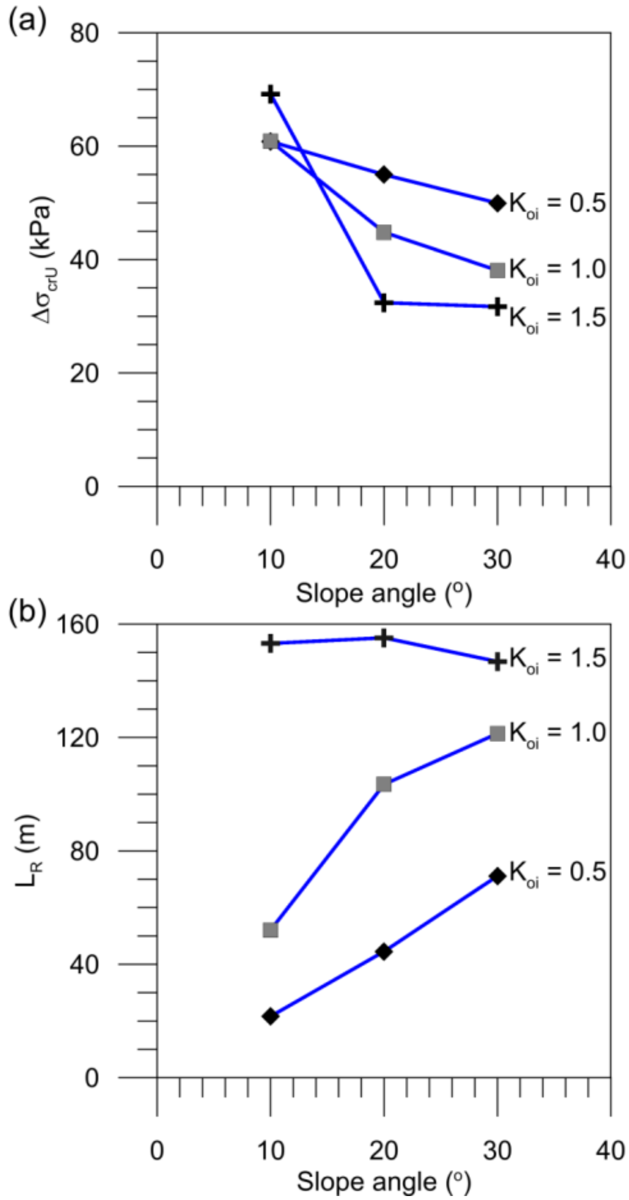

Figure 14: Influence of the slope angle on (a) the critical unloading stress initiating progressive failure ($\Delta\sigma_{crU}$) and (b) the retrogression distance (L_R) for different K_{oi} values. Slopes having a height of 20 m and peak and large deformation shear strengths of 70 and 10 kPa respectively are considered.

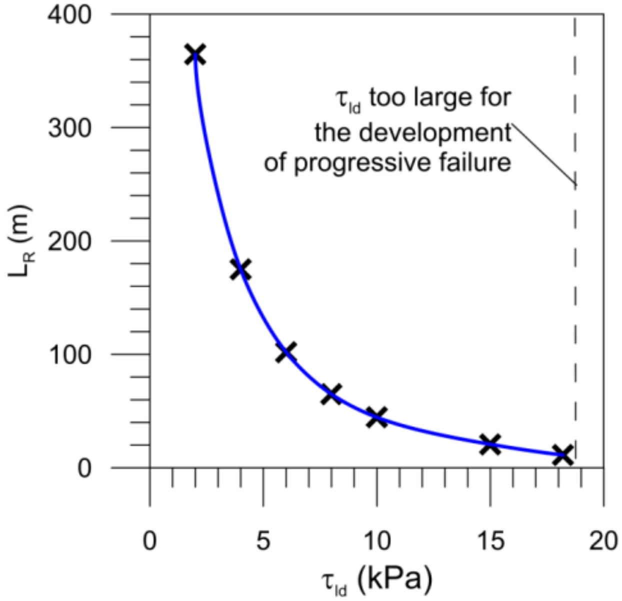

Figure 15: Retrogression distance (L_R) of the failure surface as a function of τ_{ld} for a slope inclined at 20° and having a height of 20 m, K_{oi} of 0.5 and a peak shear strength of 70 kPa.

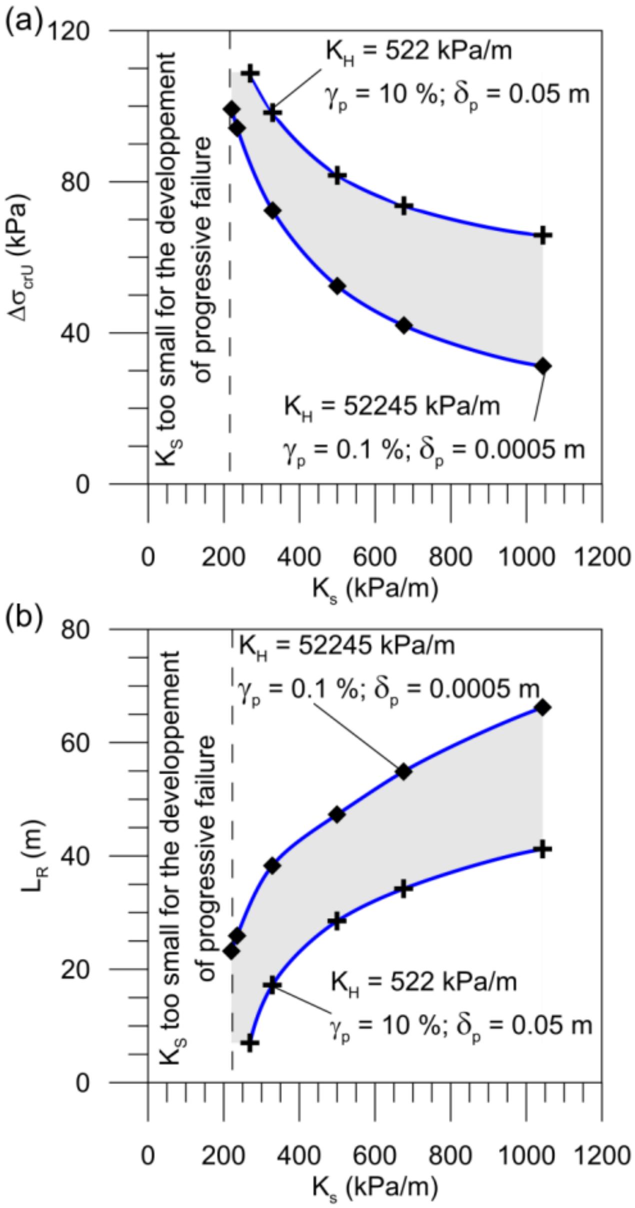

Figure 16: Influence of K_S on (a) the critical unloading stress initiating progressive failure ($\Delta\sigma_{crU}$); and (b) the retrogression distance of the failure surface during progressive failure (L_R). Shaded areas show the effect of variation of K_H. Slopes having a height of 20 m, 20° of inclination and peak and large deformation shear strengths of 70 and 10 kPa respectively are considered.

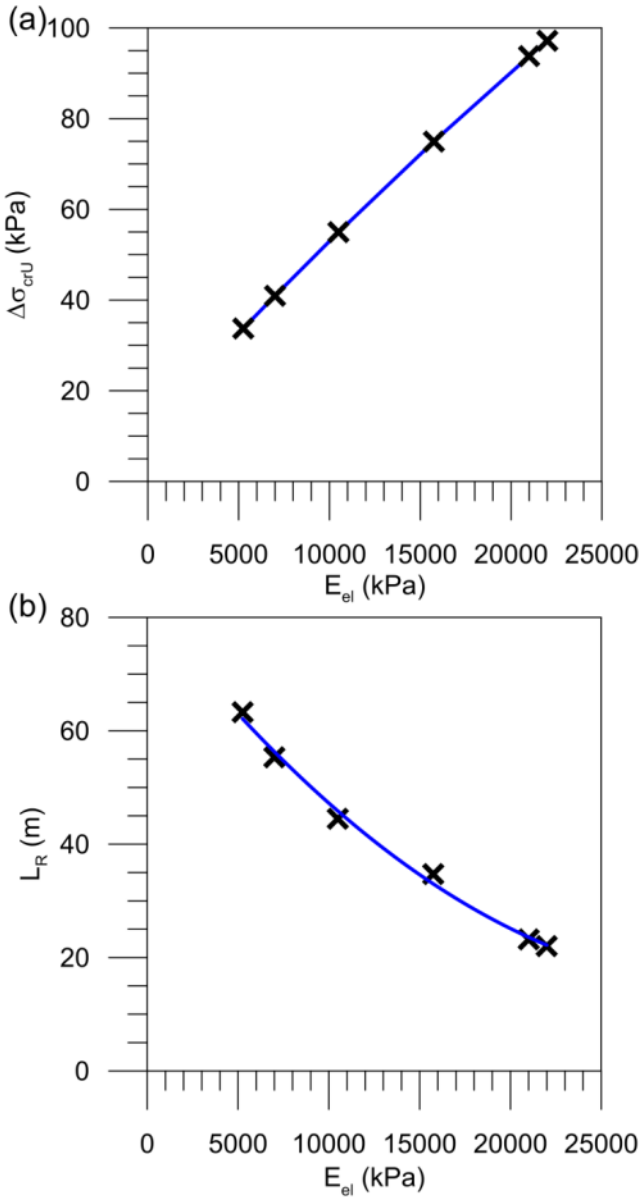

Figure 17: Effect on E_{el} on the (a) the critical unloading stress initiating progressive failure ($\Delta\sigma_{crU}$); and (b) the retrogression distance of the failure surface during progressive failure (L_R). Slopes having a height of 20 m, 20° of inclination and peak and large deformation shear strengths of 70 and 10 kPa respectively are considered.